
Depositional environment and source rock potential of Cenomanian and Turonian sedimentary rocks of the Tarfaya Basin, Southwest Morocco

B.I. GHASSAL¹ R. LITKE¹ V. SACHSE¹ S. SINDERN² J. SCHWARZBAUER¹

¹Energy and Mineral Resources Group (EMR), Institute of Geology and Geochemistry of Petroleum and Coal

Lochnerstr. 4-20, RWTH Aachen University, 52056 Aachen, Germany

Ghassal E-mail: bandar.ghassal@emr.rwth-aachen.de

²Energy and Mineral Resources Group (EMR), Institute of Mineralogy and Economic Geology

Wüllnerstrasse 2, RWTH Aachen University, 52062 Aachen, Germany

| A B S T R A C T |

Detailed organic and inorganic geochemical analyses were used to assess the depositional environment and source rock potential of the Cenomanian and Turonian oil shale deposits in the Tarfaya Basin. This study is based on core samples from the Tarfaya Sondage-4 well that penetrated over 300m of Mid Cretaceous organic matter-rich deposits. A total of 242 samples were analyzed for total organic and inorganic carbon and selected samples for total sulfur and major elements as well as for organic petrology, Rock-Eval pyrolysis, Curie-Point-pyrolysis-gas-chromatography-Mass-Spectrometry and molecular geochemistry of solvent extracts. Based on major elements the lower Cenomanian differs from the other intervals by higher silicate and lower carbonate contents. Moreover, the molecular geochemistry suggests anoxic bottom marine water conditions during the Cenomanian-Turonian Boundary Event (CTBE; Oceanic Anoxic Event 2: OAE2). As a proxy for the S_{org}/C_{org} ratio, the ratio total thiophenes/total benzenes compounds was calculated from pyrolysate compositions. The results suggest that S_{org}/C_{org} is low in the lower Cenomanian, moderate in the upper Cenomanian, very high in the CTBE (Cenomanian-Turonian Boundary Event) and high in the Turonian samples. Rock-Eval data reveal that the lower Cenomanian is a moderately organic carbon-rich source rock with good potential to generate oil and gas upon thermal maturation. On the other hand, the samples from the upper Cenomanian to Turonian exhibit higher organic carbon content and can be classified as oil-prone source rocks. Based on Tmax data, all rocks are thermally immature.

The microscopic investigations suggest dominance of submicroscopic organic matter in all samples and different contents of bituminite and alginite. The lower Cenomanian samples have little visible organic matter and no bituminite. The upper Cenomanian and CTBE samples are poor in bituminite and have rare visible organic matter, whereas the Turonian samples change from bituminite-fair to bituminite-rich and to higher percentages of visible organic matter towards the younger interval. These differences in the organic matter type are attributed to i) early diagenetic kerogen sulfurization and ii) the upwelling depositional environment. Moreover, kerogen sulfurization was controlled by the relationship between carbonate, iron and sulfur as well as the organic matter. Thus, the organic carbon-rich deposits can be grouped into: i) low S_{org} and moderately organic matter-rich oil prone source rocks, ii) moderate S_{org} and organic-carbon-rich oil prone source rocks, iii) high S_{org} and organic carbon-rich oil prone source rocks and iv) very high S_{org} and organic carbon-rich oil prone source rocks, the latter representing the CTBE interval. Types 2 to 4 will generate sulfur-rich petroleum upon maturation or artificial oil shale retorting. This integrated organic and inorganic approach sheds light on the various processes leading to the development

of the world-class oil shales deposited through the Cenomanian to Turonian. In addition, this study shows how the changes in the depositional environment might have controlled kerogen sulfurization and organic matter preservation and structure. This detailed approach provides a better understanding on source rock development during the Cenomanian to Turonian in a global context, as many of the geochemical features were identified worldwide for deposits related to OAE2.

KEYWORDS | Oceanic Anoxic Event. Oil shale. Petroleum source rock. Biomarker. Organic sulfur. Organic matter.

INTRODUCTION

The Tarfaya Basin is located in southwest Morocco, south of the Anti-Atlas with the Reguibat massif in the east, the Mauritanides Mountains in the south and the Atlantic Ocean abyssal plain in the west (Fig. 1). It is considered as one of the main petroleum basins along the eastern Atlantic coast and belongs to the major oil shale deposits in Morocco (Dyni, 2006).

Exploration activities for conventional oil increased during the 1960s and early 1970s when several wells encountered gas and oil shows. This led to a heavy oil discovery offshore in the Jurassic play (SUBSEAIQ, 2014), *ie.* the Cap Juby field. In the 1980s, Shell assessed the Upper Cretaceous (Cenomanian/Turonian)

succession in the onshore part of the basin for open pit oil shale mining; however, the deposits were regarded as non-commercial at that time (Lüning *et al.*, 2004). The estimated total oil shale resource of the Tarfaya Basin is 86 billion tons with an average thickness of the mineable deposits of 20m (Dyni, 2006) and Total Organic Carbon content (TOC) of up to 20% for the Cenomanian (Kolonic *et al.*, 2002; Sachse *et al.*, 2011, 2012, 2014). Based on a well correlation (Michard *et al.*, 2008) and an interpreted seismic line (Wenke, 2014; Fig. 2), the offshore basin differs from the onshore part, as in the offshore area a thick Tertiary succession and Triassic salt domes were identified (Fig. 2). This finding essentially increased the chance of finding more thermogenic oil and gas accumulations in the offshore area, where sufficient maturation of source rocks can be expected. In addition,

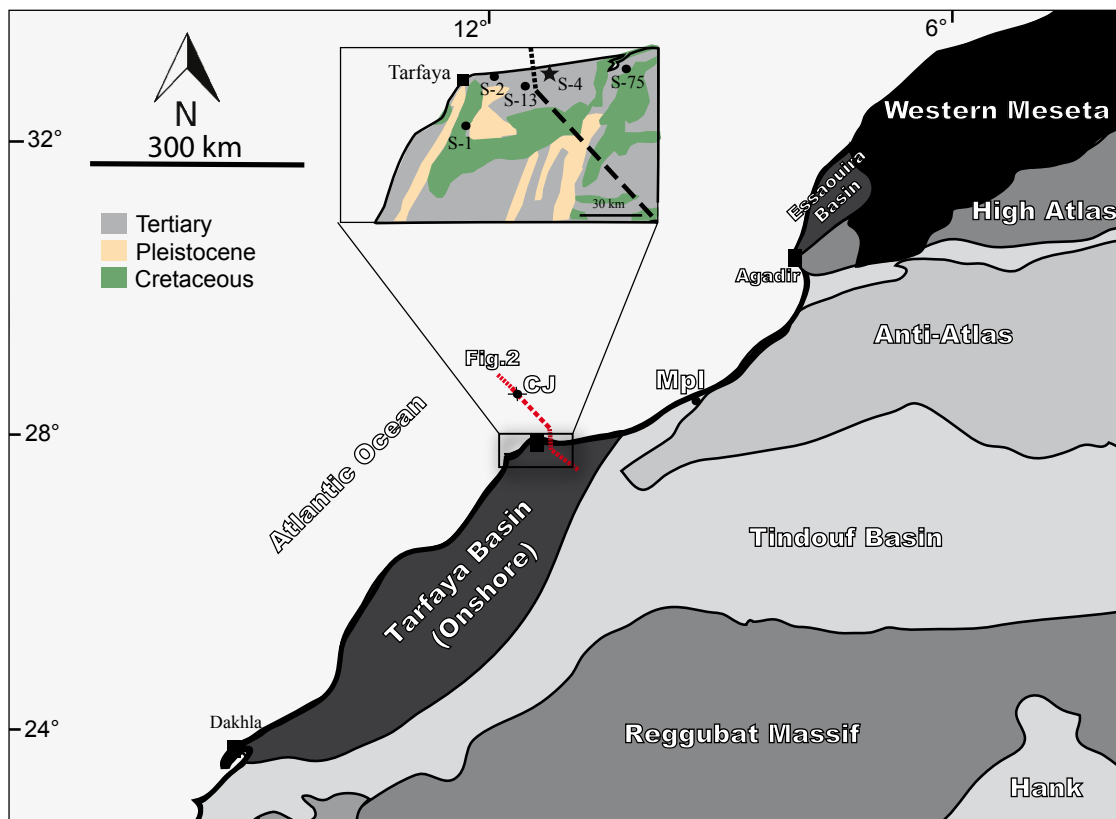


FIGURE 1. Overview map of the Tarfaya Basin showing the location of the studied well (S-4) and some of the previously studied wells (modified after Michard *et al.*, 2008). Surface geology in the small map modified after Saadi *et al.* (1985). CJ: Cap Juby well.

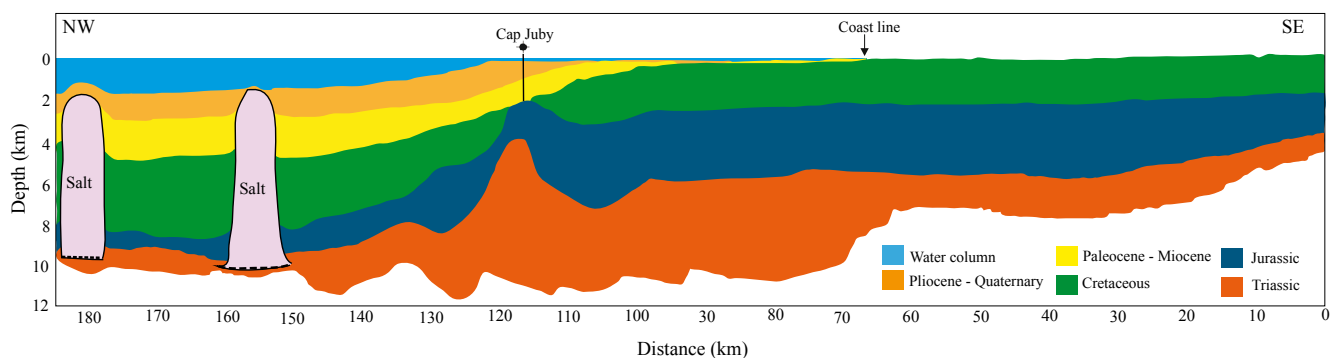


FIGURE 2. Cross section showing the extent of the onshore/offshore stratigraphy of the Tarfaya Basin (modified after Wenke, 2014), including Cap Juby well.

the Canary hotspot is situated in direct vicinity to the Tarfaya Basin and might have affected heat flow leading to mature Cretaceous source rocks (see Neumaier *et al.*, 2015), if this rocks are present on the offshore area.

Several potential reservoirs were discussed in the literature but according to offshore well data gas and oil are present in the Jurassic and Lower Cretaceous (Morabet *et al.*, 1998). The single oil discovery, Cap Juby, contains low and high API (American Petroleum Institute) gravity oil in the Lower and Middle Jurassic, respectively. Source to oil geochemical correlations suggested carbonate-rich source rocks for these oils (Morabet *et al.*, 1998). Potential seals are distributed throughout the pre-, syn- and post-rift sections with shaly and evaporitic lithologies; accordingly sealing capacity is not regarded as limiting factor for hydrocarbon accumulations.

The source rock characteristics in the Tarfaya Basin were assessed in detail by Kolonic *et al.* (2002), Lüning *et al.* (2004) and Sachse *et al.* (2011, 2012, 2014) based on outcrops and onshore wells (Fig.1).

Outcrop samples from the Devonian, Carboniferous, Jurassic and Lower Cretaceous showed poor source rock potential (Sachse, 2011). However, results published by Enachescu *et al.* (2010) indicated that the offshore oil in the Tarfaya Basin was sourced by Jurassic marly facies with TOC values ranging from 1.47 to 2.49%. On the other hand, the Upper Cretaceous embraces the highest source rock quality compared to the other stratigraphic sections in the basin. The Cenomanian and Turonian outcrop (Sachse *et al.*, 2011) and core samples (Kolonic *et al.*, 2002; Sachse *et al.*, 2012, 2014) are characterized as excellent immature oil prone source rocks, based on high values of TOC and Hydrogen Index (HI) and low to moderate values of Tmax and vitrinite reflectance. They are characterized by high Total Sulfur content (TS) but only moderate TS/TOC ratio (Kolonic, *et al.*, 2002; Sachse *et al.*, 2011, 2012, 2014). Outcrop samples from the Coniacian, Santonian,

Campanian and Eocene show similar hydrocarbon richness, maturity and generative potential (Sachse *et al.*, 2014).

The first objective of this study is to assess the source rock potential in the Cenomanian and Turonian using new core samples from SONDAGE-4 well, drilled in 2009 (Fig. 1). In addition, the study intends to determine the depositional environment as well as associated processes that led to the preservation of organic matter during the Cenomanian to Turonian times using a variety of organic and inorganic geochemical and petrographic techniques. In particular the change of organic facies through time is investigated in detail and visualized by petrographic sections. In addition, the results of this study are relevant to better understand the extent (time and space) and intensity of Oceanic Anoxic Event 2 (OAE2), and its relation to source rock deposition. Finally, the paper classifies the investigated source rocks based on several criteria that could be useful for both scientific and industrial communities.

GEOLOGICAL SETTING

The Tarfaya Basin is one of the Mid Atlantic rift basins along the northwestern African margin. Extension started in Late Permian to Early Jurassic times as a sag basin (Wenke *et al.*, 2011) leading to major faulting and northeast oriented half grabens (Lancelot and Winterer, 1980; Hafid *et al.*, 2008). The first synrift units of the Triassic were characterized by terrigenous clastics that were deposited in an alluvial environment followed by basaltic extrusives and doleritic sills (Lancelot and Winterer, 1980). Triassic salt was only observed in the northwestern part of the offshore Tarfaya Basin (Lancelot and Winterer, 1980; Hafid *et al.*, 2008). In the Early Jurassic, major transgressions switched the basin to a marine system (Wenke *et al.*, 2011). Carbonates and evaporites were deposited at the beginning of the Early Jurassic along the Moroccan margin. Moreover, the Early Jurassic witnessed tectonic instability due to the initiation of continental drifting (Lancelot and

Winterer, 1980). This tectonic setting was responsible for the development of carbonate ramps in the Early- to Mid-Jurassic followed by regressive marine siliciclastic environments. Transgression occurred again in the early Late Jurassic and led to the deposition of open marine carbonates (Wenke *et al.*, 2011; Hafid *et al.*, 2008). The depositional environment changed in the Middle Jurassic giving rise to carbonate platforms and build-ups (Wenke *et al.*, 2011). Regression took place again in the Late Jurassic/ Early Cretaceous, shifting the depositional environment to lagoonal and deltaic (Hafid *et al.*, 2008). The basin at this time included two depositional environments: deltaic facies dominated the northern area and prograded to the NNE, whereas the northwestern and southern areas encountered outer shelf carbonates to fine-grained clastic deposits (Wenke *et al.*, 2011). The Lower Cretaceous is composed of shales, sandstones and shelly limestones with occasional organic matter-rich units and can reach a thickness of up to 1700m (Einsele and Wiedmann, 1982; Morabet *et al.*, 1998). The Albian witnessed sea level fluctuations and is characterized by variable lithologies from open marine carbonates to silty clays and marls (Lancelot and Winterer, 1980; Einsele and Wiedmann, 1982; Wenke *et al.*, 2011). Furthermore, deep sea drilling penetrated organic rich beds in the northern offshore basin (Einsele and Wiedmann, 1982). Several transgressive-regressive cycles might have occurred in the Albian/Cenomanian, Cenomanian/Turonian and Santonian/Campanian (Kolonic *et al.*, 2002). The highest organic carbon content is thought to be associated with these transgressions (Morabaet *et al.*, 1998). The greatest sea level rise occurred coeval with the OAE2, the Cenomanian/Turonian Boundary Event (CTBE) (Schlanger and Jenkyns, 1976; Jenkyns, 1980). This major transgression affected the North Africa all the way to the Sahara platform (Lancelot and Winterer, 1980) leading to deposition of organic matter-rich clays and marls in a nutrient-rich warm water environment (Erbacher *et al.*, 1996; Kolonic *et al.*, 2002). Sachse *et al.* (2014) pointed out that the influence of reduced oxygen content due to lower oxygen solubility in water at high temperature triggered the organic matter preservation. The uppermost Cenomanian as well as the Turonian succession are laminated unlike the lower Cenomanian and Lower Cretaceous (Einsele and Wiedmann, 1982).

A major unconformity exists between the late Santonian and the Paleogene (Lancelot and Winterer, 1980; Hafid *et al.*, 2008; Wenke *et al.*, 2011). The Upper Cretaceous is thin or missing and unevenly distributed in the shallow water areas as shown in Figure 2. Interestingly, most of the Upper Cretaceous sediments are also eroded or undrilled in the Tarfaya deep water area. Another important transgression occurred in the Eocene resulting in upwelling and related high surface water productivity leading to deposition of organic matter-rich units (Sachse *et al.*, 2014). This was

followed by a time of non-deposition during the Early Oligocene (Lancelot and Winterer, 1980). Furthermore, the uplift of the Canary island volcanic region during the Miocene shifted the depocenter towards the abyssal part of the basin (Kuhnt *et al.*, 2009). Finally, the latest stratigraphic section recorded in the Tarfaya is the Miocene Moghrebien Formation (Kolonic *et al.*, 2002). Figure 2 is a cross section representing the distribution of the various stratigraphic units in the onshore and offshore areas. The most common lithologies are summarized in a generalized stratigraphic column (Fig. 3).

SAMPLES AND METHODS

Samples

A total of 242 core samples were collected from Tarfaya Sondage-4. The well was drilled in 2009, located 40km east of Tarfaya (N27°59'46.4", W12°32'40.6") as part of a drilling campaign in order to recover the Miocene to Albian sequences. The borehole has a total depth of 350.20m with 100% sediment recovery. It penetrated 21.00m of the Miocene Moghrebien Formation, 79.00m of the Turonian, and 15.06m covering the CTBE interval, 163.04m of the upper Cenomanian and 72.1m of the lower Cenomanian and Albian section. The CTBE in this well was described in Schönfeld *et al.* (2015) where C isotope excursions were discussed. The boundary between the Lower and upper Cenomanian was tentatively based on changes in geochemical features. Detailed sedimentological and micropaleontological studies on the same well are currently conducted by the marine micropaleontology group at Christian-Albrechts University, Kiel, Germany. The two deepest samples were assigned to the Albian, but they are not discussed in detail due to their small number.

Elemental Analysis

For geochemical analysis, all samples were powdered, whereas small pieces were preserved for microscopic studies. All samples were analyzed for Total Organic and Inorganic Carbon (TOC and TIC) using a LiquiTOC II (Elementar Analysengeräte GmbH). The analytical method is described in Bou Daher *et al.* (2015). The CaCO₃ proportion was calculated using the equation: CaCO₃=inorganic carbon x 8.333. This calculation has to be used with caution as it will result in overestimation of carbonate contents (by up to 8%) if dolomite is present instead of calcite.

TS was measured on 162 samples: 15 samples from the lower Cenomanian, 44 from the upper Cenomanian, 83 from the interval comprising the CTBE and 20 from the

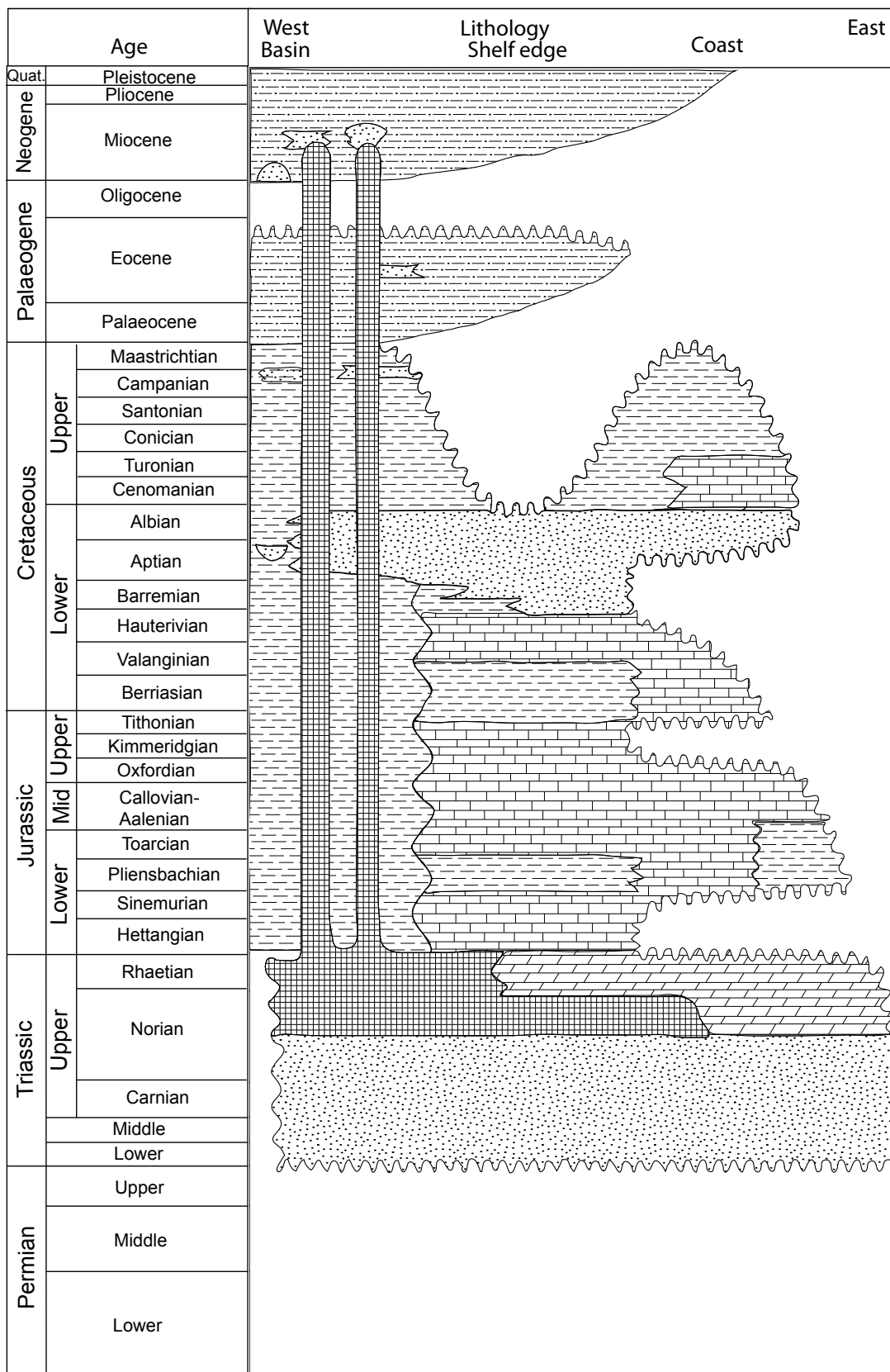


FIGURE 3. Stratigraphic column representing the common lithologies in the Tarfaya Basin from coastal to deep marine areas (modified after Davison, 2005; Seht, 2014).

Turonian. TS was measured using a LECO S 200 sulfur analyzer (precision is <5% and detection limit 0.001%).

Based on CaCO₃ and TS values as well as pyrolysis data, 20 samples were selected for determination of major element concentrations: 5 from the lower Cenomanian, 6 from the upper Cenomanian, 5 from the CTBE and 4 from the Turonian. Approximately 2g of powdered rock of each sample was put overnight into an oven at 105°C to dry. Then, the samples were weighed and placed in an oven at 1000°C for 2 hours for loss of ignition (LOI) process. After that, the samples were left to cool in moisture-free atmosphere and weighed again to calculate the loss on ignition. Next, the samples were mixed with a Li-tetraborate/Li-metaborate mixture (FX-X65, Fluxana, Kleve, Germany) with a ratio of 0.5g/5g. The mixture was fused at 1150°C to create a glass disc to be used for major element analysis by energy dispersive X-ray fluorescence spectrometry (Spectro XLab2000). The system has a Pd-tube operated at acceleration voltages between 15 and 40kV and currents between 6 and 12.0mA. Secondary targets of Co, Ti and Al were used for signal enhancement. A fundamental parameter procedure was applied for data computation. The precision of major element determination was <0.9%.

Rock-Eval Pyrolysis

Rock-Eval pyrolysis analyses were conducted on 99 core samples to characterize their source rock potential using a Rock-Eval 6. The method is described in Espitalié *et al.* (1985) and Peters (1986). Samples cover the lower Cenomanian (14), upper Cenomanian (19), the CTBE interval (38) and Turonian (26). Various parameters were used from Rock Eval data. S1 (mgHC/gRock) represents the free hydrocarbons and S2 (mgHC/gRock) represents the non-soluble hydrocarbons with organic solvents (mostly kerogen). S3 represents the CO₂ released from hydrocarbon during pyrolysis (mgCO₂/gRock). Hydrogen Index (HI; S2/TOC; mgHC/gTOC) and Oxygen Index (OI; S3/TOC; mgCO₂/gTOC) were calculated as common parameters to describe the quality of the source rock with respect to petroleum generation. Finally, the Production Index (PI) has been calculated as follows: S1/(S1+S2). All pyrograms were checked carefully for good S2 peak developments for quality control. Note that none of the Rock Eval samples have TOC lower than 0.5% or S2 lower than 1.5mgHC/gRock. Therefore, values of all parameters including T_{max} and HI are believed to be accurate.

Organic petrology

Maceral counting was performed on 32 samples to investigate the organic petrological changes through the studied interval. 4 samples were from the lower Cenomanian, 6 from the upper Cenomanian, 14 from

the CTBE and 8 from the Turonian. The petrological study used the methods described by Taylor *et al.* (1998). The bulk samples were cut and embedded perpendicular to bedding, in a 10:3 mixture of epoxy resin (Araldite® XW396), and hardener (Araldite® XW397) and dried at 37°C for at least 12 hours. The sample surfaces were then grinded and polished as described in detail by Sachse *et al.* (2012). On each bulk sample a total of at least 500 maceral counts were performed. Counting was performed both in incident white light (for vitrinite and inertinite, and also pyrite) and in a fluorescent light mode (for bituminite, telalginite, lamalginite, and liptodetrinite) along transects perpendicular to bedding.

The percentage of each category (as OM volume-% of whole rock) was calculated and finally the percentages of all macerals were determined. The maceral percentages were compared with the volume percentage of organic matter based on TOC-content. This estimation is based on the equation introduced by Littke (1993) which is:

$$\text{TOC (wt\%)} = (\text{qOM/qrock}) \times (\text{C\%/100}) \times \text{OM (vol.\%)}$$

Where C% is the carbon content of the Organic Matter (OM). The difference between the calculated OM from the equation and the counting should correspond to the amount of submicroscopic OM.

Source rock extraction

For a total of 24 source rocks aliquots of 3 to 7g of powdered samples were extracted. To each sample, 50mL of dichloromethane (DCM) were added and agitated in an ultrasonic bath for 15 minutes. Thereafter, the solution was stirred overnight at room temperature. Then, the solution was agitated again in an ultrasonic bath for 15 minutes. After filtration, copper powder was added to remove elemental sulfur. Using a liquid chromatography micro column (Baker, filled with 2g of silica gel 40mm), the raw extracts were separated into 6 fractions of increasing polarity using n-pentane (5ml), n-pentane/DCM 95/5 v/v (8.5ml), n-pentane/ DCM 90/10 v/v (5ml), n-pentane/DCM 40/60 v/v (5ml), DCM (5ml) and methanol (5ml), respectively. The fractionation method is described in detail in Schwarzbauer *et al.* (2000). For Gas Chromatography-Mass Spectrometry (GC-MS) analyses the first fraction containing the aliphatic hydrocarbons was used.

Gas Chromatography and Gas Chromatography-Mass Spectrometry

The aliphatic fractions were analyzed by gas chromatography using a Fisons Instruments GC 8000 series equipped with a flame ionization detector and a Zebron ZB-1 HT Inferno fused silica column (30m x

0.25mm internal diameter (i.d.); film thickness 0.25 μ m, Phenomenex®). Each sample was concentrated to approximately 25–50 μ L prior to injection. 1 μ L was injected into a split/splitless injector at 270°C and with a splitless time of 60s. Helium was utilized as a carrier gas with a gas velocity of 35cm/s. The temperature program started at 80°C, held for 3 minutes; then the temperature increased at a rate of 10°C/minute to reach 300°C remaining constant for 20 minutes. The aliphatic fractions were further analyzed on a Finnigan MAT 95 mass spectrometer connected to a Hewlett Packard Series II 5890 GC which was equipped with a similar GC column. The carrier gas was He with a gas velocity of 33cm/s. The GC run started at 80°C, held for 3 minutes; then the temperature increased to 310°C at a rate of 5°C/minute. The spectrometer was operated in Electron Ionization (EI*) mode with an ionization energy of 70eV and a source temperature of 200°C. The scanning range was from m/z 35 to 700 in low resolution mode.

Curie-Point Pyrolysis Gas Chromatography-Mass Spectrometry

A total of 18 samples (4 from the lower Cenomanian, 4 from the upper Cenomanian, 4 from the CTBE interval and 6 from the Turonian) were selected for Curie-Point pyrolysis coupled to a GC-MS system (CP-PyGC-MS), based on TOC and TS contents. Metal crucibles with Curie Point temperature of 650°C were made in the lab. Then, each crucible was filled with 3 to 10mg of powdered sample. The crucible was inserted in a glass inlet which was then placed in a CP pyrolyzer (Fischer GSG CPP 1040 PSC) and pyrolyzed at 650°C for 10s. The pyrolyzer was coupled up to a GC-MS system (Fisons GC 8000; Thermoquest MD 800). It was equipped with a 30m non-polar GC capillary column (Zebron ZB-5, 0.25mm i.d., 0.25 μ m film thickness). The pyrolysis products were trapped behind the injector using a cryofocussing trap (-70°C) prior to the GC-MS analyses. The GC-MS analyses were conducted using He as carrier gas (velocity 35cm/s) and 40°C as starting oven temperature held for 3 minutes. Then the oven temperature increased at a rate of 3°C/minute to reach 310°C held for 20 minutes. Molecular masses were scanned from m/z 35 to 550.

Molecular geochemical parameters

All biomarker ratios were calculated on the base of peak integration of specific ion chromatograms. For alkanes such as n-C₁₇, n-C₁₈, pristane and phytane ion chromatograms of m/z 57 were used. Hopanes and methylated derivatives were determined with m/z 191 and 205, respectively. C₂₇, C₂₈ and C₂₉ steranes were measured at m/z 217 trace but checked with the ion chromatograms of the molecular ions. In summary, the following biomarker ratios were calculated: pristane/phytane (Pr/Ph), pristane/n-C₁₇ and

phytane/n-C₁₈ ratios, as well as methylated hopanes/total hopanes and steranes/hopanes ratios. As a proxy for the ratio of organic sulfur to organic carbon the thiophene/benzene ratio was calculated (thiophenes/benzenes). The thiophene derivatives considered in the equation were: methylthiophenes (2 isomers, m/z 98), dimethylthiophenes (4 isomers, m/z 112) and trimethylthiophenes (3 isomers, m/z 126). The benzene derivatives used in the equation were: toluene (m/z 92), xylenes (3 isomers, m/z 106) and trimethylbenzenes (2 isomers, m/z 120).

RESULTS

Elemental Analysis

Variable TOC content was found throughout the analyzed section (Table I; Fig. 4) ranging from 0.72 to 4.54% in the lower Cenomanian. The upper Cenomanian samples show higher values increasing towards the CTBE interval with an average of 5.50%. The CTBE interval between 100 and 115m depth shows strong fluctuations between 1.71 and 15.44% with highest values towards the top and an average of 8%. Similarly the Turonian section is characterized by high TOC values ranging from 1.69 to 15.36% and decreasing towards the top (Fig. 4).

TS content generally increases from the bottom to the top of the analyzed section (Fig. 4). The lower Cenomanian shows the lowest TS content with an average of 0.8% and values varying between 0.4 and 1.5%, whereas the upper Cenomanian samples average 1.3% and range from slightly less than 1% to 2.2% with highest values towards the CTBE. The CTBE samples show strong fluctuations in sulfur with highest values towards the top (4.3%) and average value of 1.5%. The Turonian is also characterized by a high TS average of 1.9%.

The carbonate content oscillates rapidly and appears to have a relationship with the TOC and TS contents (Table I; Fig. 4). The lower Cenomanian samples have relatively low to moderate CaCO₃ content, compared to the younger intervals, with an average of 41%. The upper Cenomanian samples on the other hand start with moderate carbonate content which increases toward the CTBE to exceed 60% on average. The CTBE and Turonian samples are very rich in carbonate with an average of more than 68%. However, these stratigraphic levels also have five narrow low CaCO₃ intervals (<50%). In general, the samples show an inverse correlation between CaCO₃ and TS. The same holds true for the CaCO₃ vs. TOC relationship with the exception of the lower Cenomanian (Fig. 5).

The Fe₂O₃, SiO₂, Al₂O₃, K₂O and TiO₂ contents increase with well depth, reaching highest values within

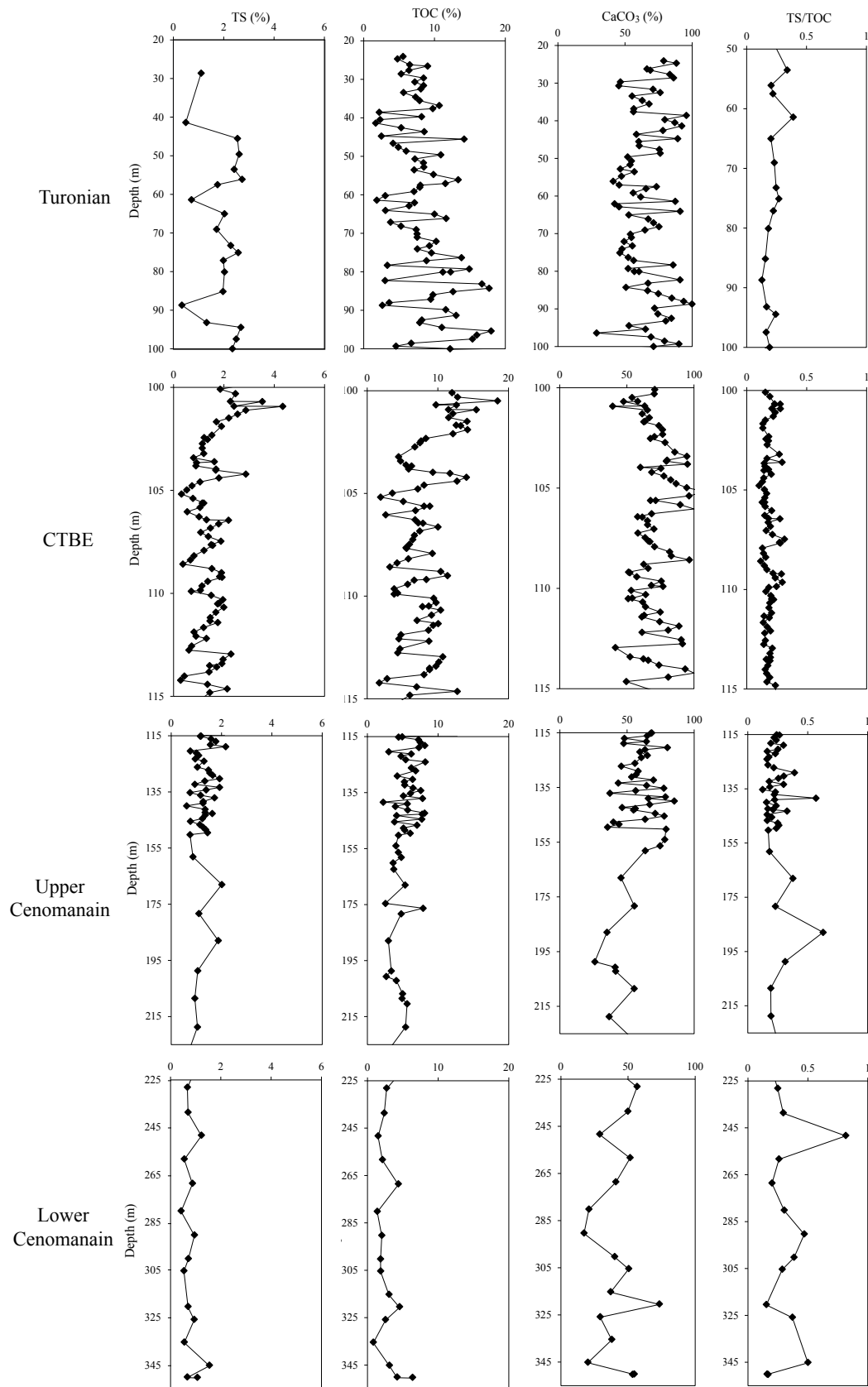


FIGURE 4. Depth plots TS, TOC, CaCO₃ and TS/TOC ratio of all stratigraphic units.

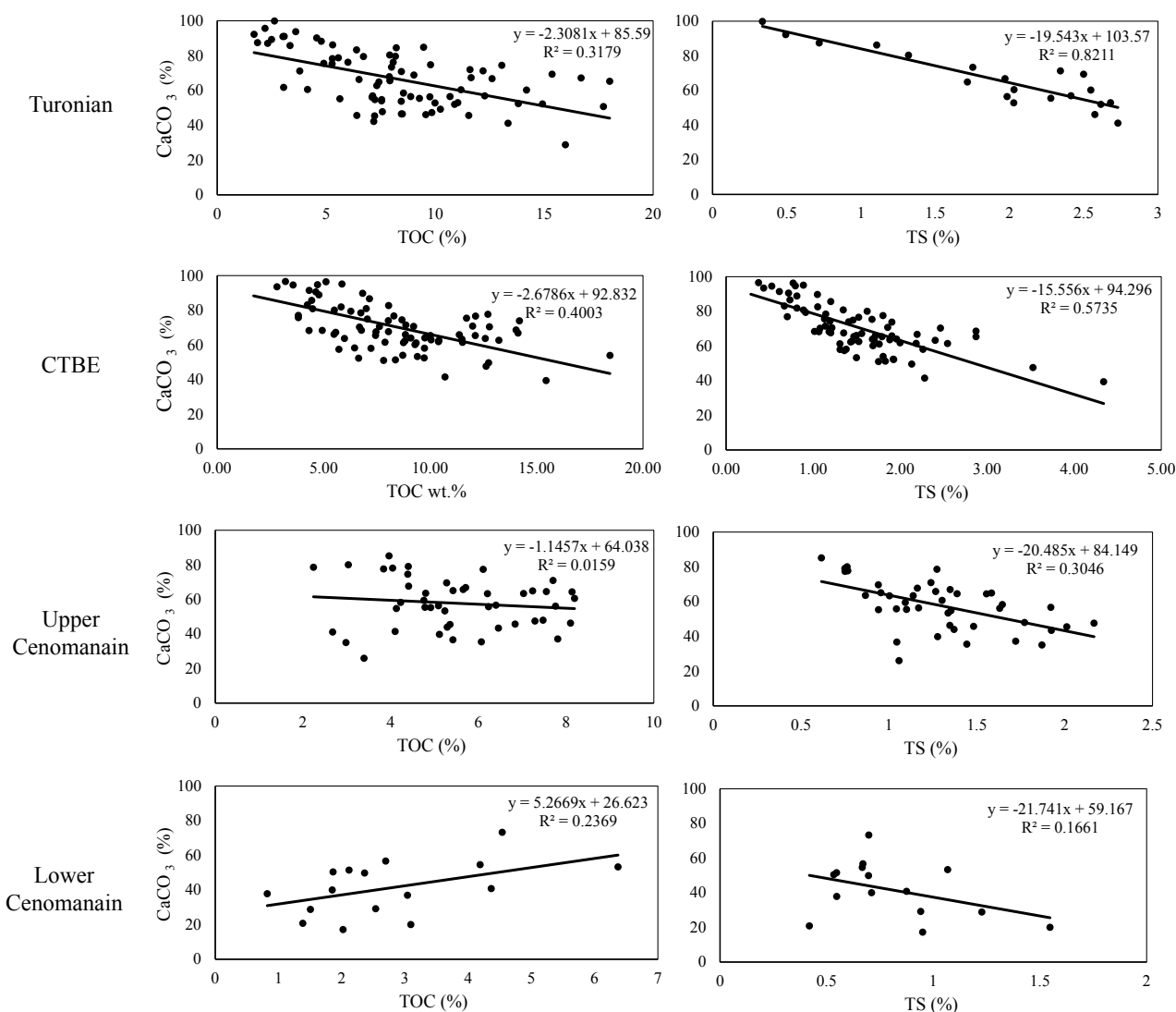


FIGURE 5. Cross plots between CaCO₃ versus TOC and TS. The correlation of CaCO₃ and TOC relationship changes significantly from positive in the Lower Cenomanian to negative in the Turonian. The CaCO₃ and TS correlations are always negative with variable regression coefficients.

the lower Cenomanian (Table II; Fig. 6) whereas CaO, SO₃ and LOI generally decrease with depth. Fe₂O₃ ranges from 2.8 to 5.1% in the lower Cenomanian and from 1.0 to 4.8% in the upper Cenomanian. A lower range is found in the samples representing the CTBE (0.1 to 3.6%). The Turonian has an even narrower range from 0.1 to 1.5%. The Fe₂O₃ and TiO₂ show a negative relationship when they are plotted against CaCO₃ (Fig. 7), which is in line with the decrease of CaO with depth. MnO is very low throughout the well and does not exceed 0.04%. MgO is relatively low but exceeds 3% in three samples (53.52m, 129.04m and 187.92m). The overall high Ca/Mg ratio indicates that carbonates are mainly present as calcite/aragonite and not as dolomite. Accordingly the calculation of calcium carbonate content from total inorganic carbon (see elemental analysis method section) is valid for almost all samples. P₂O₅ shows high values

only at 168.00m (1.5%) and at 220.57m (1.8%). More details are given in Figure 6 and Table II.

Rock-Eval Pyrolysis

Generally two groups can be distinguished along the analyzed sections (Table I; Fig. 8). The first group includes the majority of the lower Cenomanian samples, which show moderate to high HI values (208–543mgHC/gTOC) whereas the rest of the samples compose the second group displaying high to very high HI values of more than 600mgHC/g TOC. The Lower Cenomanian reveals the highest OI compared to the other stratigraphic intervals, ranging from 32 to 176mgCO₂/gTOC and averaging 67mgCO₂/gTOC. Tmax is low with an average of 420°C (Fig. 8). Most samples plot between Kerogen type II and III when

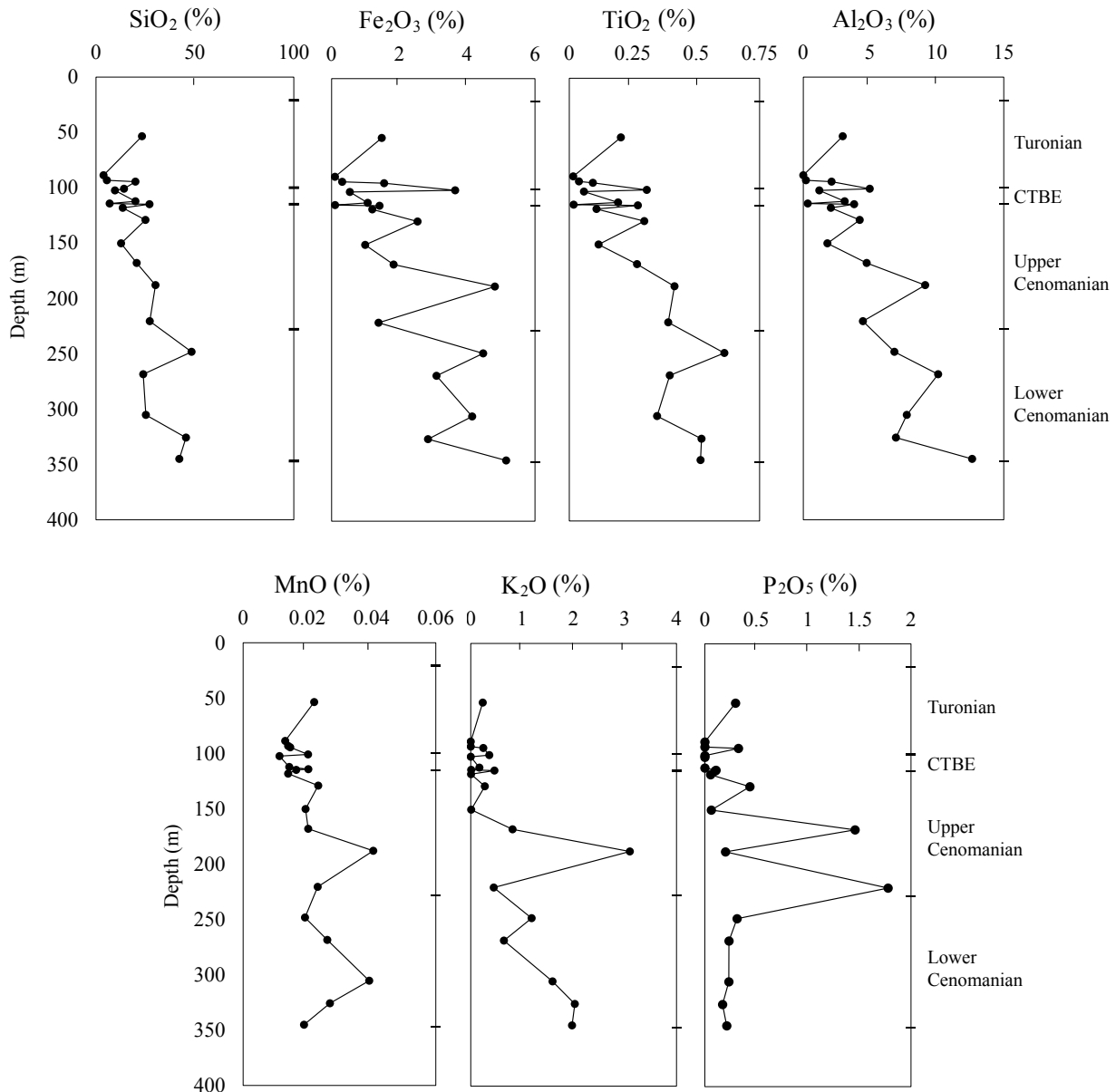


FIGURE 6. Elemental data versus depth shows increase in silicate and rutile forming elements with depth. It also shows a strong increase in P₂O₅ before the CTBE.

using the pseudo van Krevelen diagram (van Krevelen, 1950; Peters, 1986) (Fig.8).

The upper Cenomanian samples are characterized by low S1 values, similar to the lower Cenomanian, but clearly higher S2 values averaging 38.7mgHC/g rock. Moreover, the OI and Tmax average 32mgCO₂/gTOC and 416°C, respectively. Higher S1 and S2 values are observed in the CTBE samples (average of 1mgHC/g rock and 55mgHC/g rock, respectively), whereas Tmax values are low with an average of 412°C. The thick Turonian section is also composed of sediments having high HI, S1 and S2 values. S2 decreases toward the younger sediments and

Tmax averages 411°C (Fig.9). Most of the samples plot between Kerogen type I and II in the pseudo van Krevelen diagram (Fig.8)

Organic Petrology

The maceral counting reveals at least 4 different organic facies all dominated by marine organic matter (Table 1; Fig. 10). All samples show a dominance of submicroscopic Unstructured Organic Matter (UOM) with alginites/liptodetrinites constituting the majority of the visible macerals (Figs. 10; 11). These macerals show strong yellow fluorescence and are classified based on their

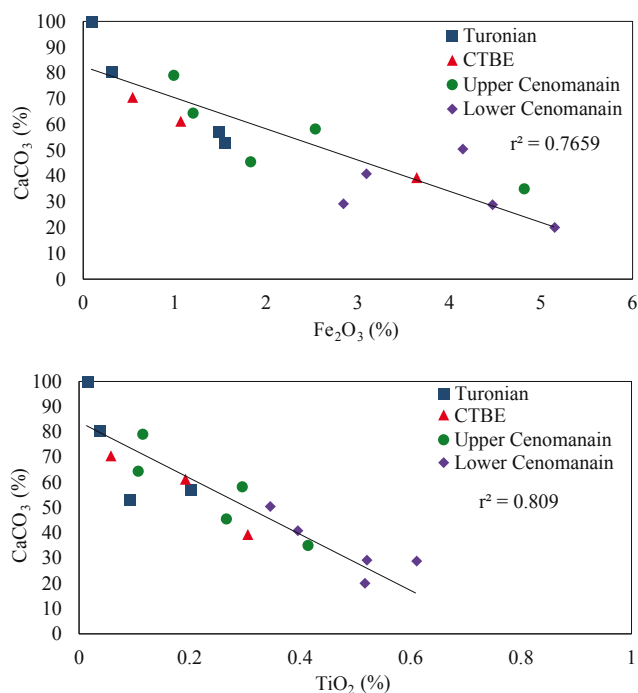


FIGURE 7. CaCO_3 versus Fe_2O_3 and TiO_2 Cross plots show inverse relationship in all studied intervals.

morphology: i) litptodetrinite (granular particle usually of less than $5\mu\text{m}$ in length), ii) lamalginate (thin elongated particles) and iii) telalginate (well preserved oval algal particles that originate from large colonial or thick walled unicellular algae; Hutton 1987, Senftle *et al.*, 1993; Taylor *et al.*, 1998).

Bituminite differs from alginite by the lack of recognized shape and reddish to dark brown fluorescence (Teichmüller and Ottenjann, 1977; Taylor *et al.*, 1998). Bituminite occurs in form of lenses of irregular shape (bituminite I) and as matrix bituminite which merges with the groundmass (bituminite II) both showing a dark, reddish fluorescence (Creaney, 1980; Taylor *et al.*, 1998). In this study bituminite II constitutes the major bituminite maceral. UOM is present to a great extent in a form that cannot be recognized by incident light microscopy, *ie.* size is smaller than $1\mu\text{m}$. The strong fluorescence of the groundmass indicates the presence of this submicroscopic organic matter.

The lower Cenomanian differs from the younger samples in the lack of bituminite (Fig. 10). It shows a strong bright yellow fluorescing ground mass. The Turonian samples are moderate in reddish groundmass and have nearly no visible organic matter. Similar characteristics are found in the samples representing the CTBE, but with more reddish groundmass and bituminite. The Turonian samples are enriched in bituminite, with rapid increase towards the

younger samples. Similarly the alginite macerals are most abundant in the younger samples. Vitrinite and inertinite are very rare throughout the investigated section with a relative increase in the lower Cenomanian samples. But even combined they do not exceed 1vol-%.

In summary, the microscopic observation classifies the source rock into 4 types which are: i) bituminite-free source rock with yellowish fluorescing submicroscopic OM (characterizes the lower Cenomanian), ii) bituminite-fair source rock with rare alginite and weak reddish fluorescing submicroscopic OM (characterizes the upper Cenomanian to lower Turonian), iii) source rock with no visible OM (characterizes few samples representing the CTBE), and iv) bituminite-rich with fair visible OM and strong reddish fluorescing submicroscopic OM.

Molecular Geochemistry

Almost all samples analyzed showed pristane and phytane predominance over the adjacent n-alkanes. The samples representing the CTBE show elevated $n\text{-C}_{16}$ to $n\text{-C}_{19}$ and low pristane/phytane (Pr/Ph) ratios, lower than in the other intervals (Fig. 12). The samples also show

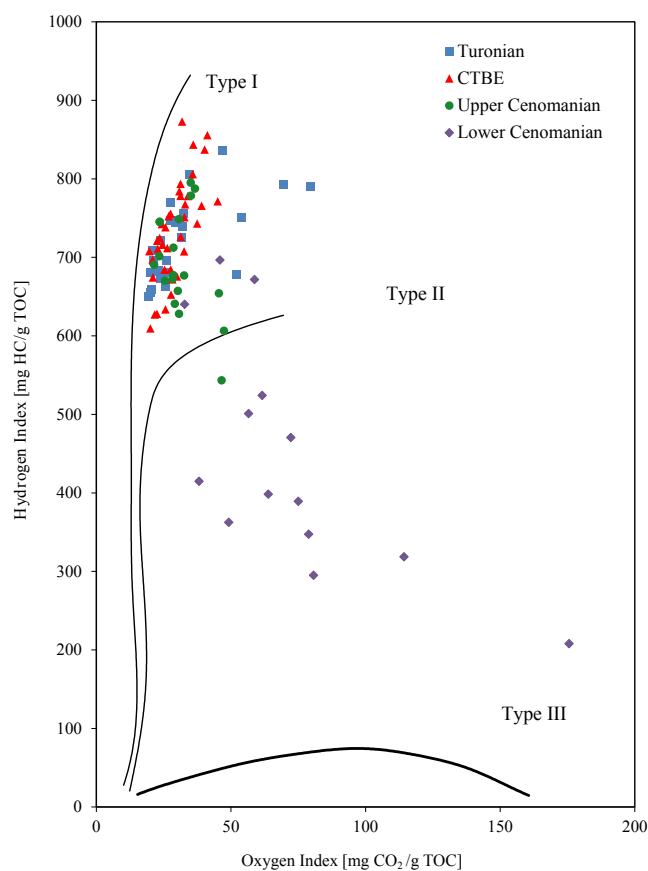


FIGURE 8. Pseudo van Krevelen diagram of bulk Rock Eval-6 samples of the various stratigraphic intervals.

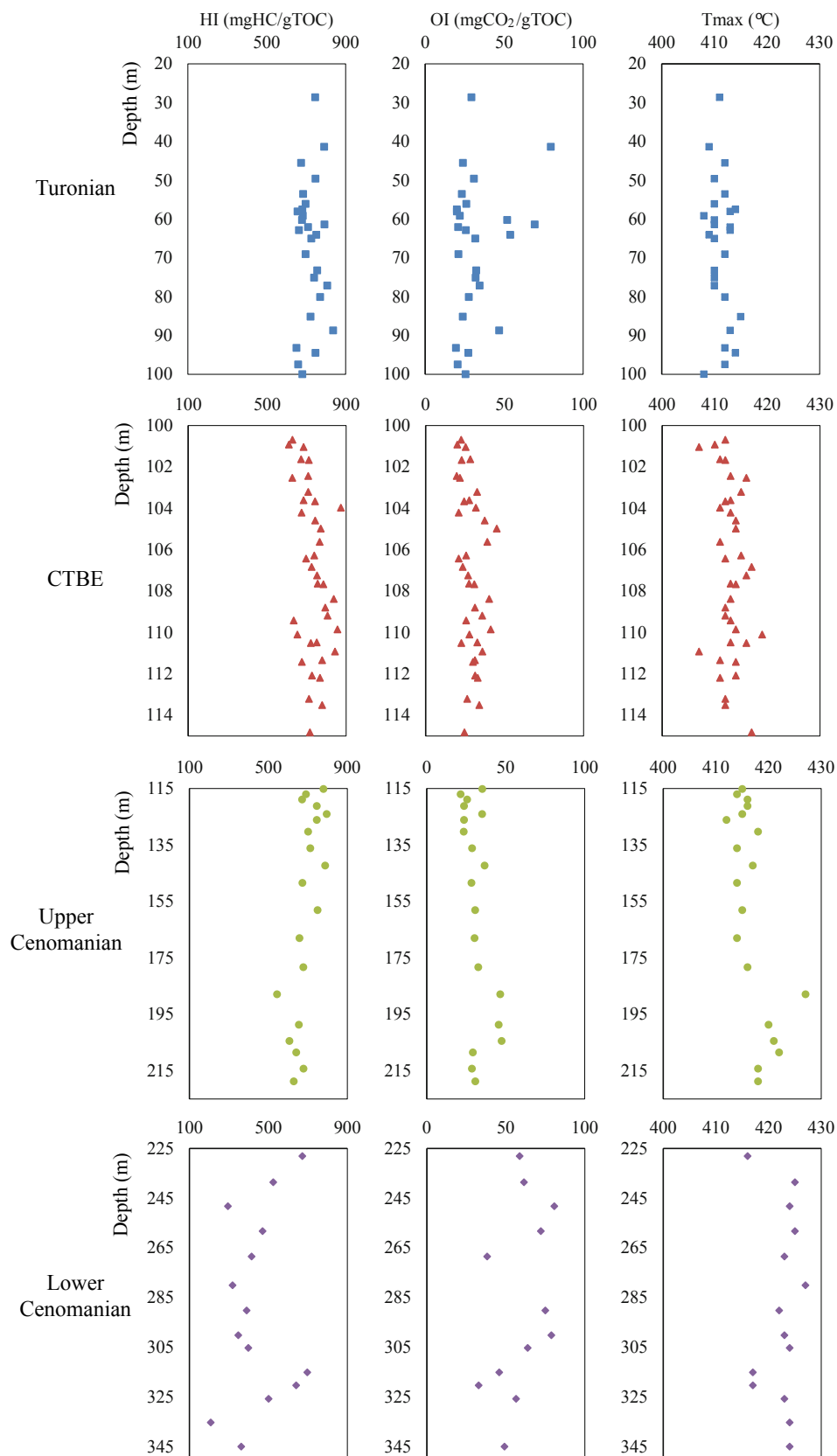


FIGURE 9. Rock Eval HI, OI and T_{max} versus depth plot. It shows the apparent difference between the Cenomanian to Turonian source rocks. On the basis of microscopic observations the T_{max} shift is interpreted to be caused by a change in the organic facies rather than thermal maturity.

TABLE 1. Maceral compositional analysis data. **: Calculated, submicroscopic organic matter

Sample	Depth (m)	Age	TOC (wt. %)	Liptodetrinite (vol.%)	Lamalginitite (vol.%)	Telalginitite (vol.%)	Bituminite II (vol.%)	UOM ** (vol.%)
14/1052	28.6	Turonian	5.30	1.47	0.47	0.07	3.89	11.30
14/1069	45.53	Turonian	14.19	0.57	1.78	0.09	6.98	36.64
14/1079	56.09	Turonian	13.34	1.37	0.70	0.09	7.88	33.27
14/1089	65.02	Turonian	9.99	0.42	0.80	0.05	7.92	23.24
14/1099	75.09	Turonian	9.57	1.32	0.54	0.04	8.44	20.71
14/1109	85.15	Turonian	12.61	2.22	0.63	0.04	9.16	28.89
14/1121	97.46	Turonian	15.36	3.40	1.43	0.05	1.18	43.83
14/1124	99.98	Turonian	12.20	2.89	1.45	0.13	1.64	33.49
14/782	100.92	CTBE	15.44	1.36	1.09	0.08	0.42	47.19
14/704	101.7	CTBE	13.23	0.00	0.00	0.00	0.00	42.95
14/783	101.67	CTBE	12.59	0.78	0.63	0.00	1.37	38.09
14/784	102.44	CTBE	7.62	0.69	0.76	0.09	1.40	21.79
14/785	103.66	CTBE	6.27	0.00	0.00	0.00	0.00	20.37
14/786	103.97	CTBE	9.29	0.15	0.21	0.05	0.67	29.07
14/787	105.62	CTBE	8.86	0.00	0.00	0.00	0.00	28.77
14/788	106.43	CTBE	7.22	0.00	0.00	0.00	0.00	23.45
14/789	107.64	CTBE	5.48	0.00	0.00	0.00	0.00	17.81
14/790	107.92	CTBE	9.22	0.00	0.00	0.00	0.00	29.95
14/791	109.19	CTBE	8.37	0.00	0.00	0.00	0.00	27.17
14/792	110.48	CTBE	8.71	0.00	0.00	0.00	0.00	28.28
14/793	111.34	CTBE	10.04	0.00	0.00	0.00	0.00	32.60
14/795	113.51	CTBE	8.82	0.00	0.00	0.00	0.00	28.62
14/585	116.11	Upper Cenomanian	7.24	0.92	0.78	0.09	0.73	20.97
14/590	121.18	Upper Cenomanian	6.21	0.00	0.00	0.00	0.00	20.15
14/623	158.11	Upper Cenomanian	4.80	0.00	0.00	0.00	0.00	15.57
14/633	178.3	Upper Cenomanian	4.78	0.00	0.00	0.00	0.00	15.52
14/648	208.5	Upper Cenomanian	4.91	0.00	0.00	0.00	0.00	15.94
14/658	228.07	Upper Cenomanian	2.70	0.00	0.00	0.00	0.00	8.75
14/673	258.24	Lower Cenomanian	2.12	0.00	0.00	0.00	0.00	6.87
14/689	290.23	Lower Cenomanian	2.02	0.00	0.00	0.00	0.00	6.56
14/771	320.34	Lower Cenomanian	4.54	0.00	0.00	0.00	0.00	14.73

elevated concentrations of methylated hopanes (C_1 -Hop) that coelute with non-methylated hopanes, and a fair percentage of C_1 -Hop that averages ~20% (of total hopanes) decreasing towards the younger samples (Table 2). The C_{27} , C_{28} and C_{29} steranes show similar characteristics and equal proportions for all samples, plotting within a narrow area (Fig. 13). The C_{28}/C_{29} steranes ratio varies slightly throughout the section but never exceeds 1.05. All samples show sterane/hopane ratios greater than 1% except for two samples at the top of the section.

Curie-Point-Pyrolysis Gas Chromatography-Mass Spectrometry

All samples show an elevated abundance of thiophenes (Table 3). The thiophenes/benzenes ratio shows very low values for the lower Cenomanian (0.98) then it increases to peak during the CTBE (8.06) and decreases slightly throughout the Turonian with values above 5.00.

DISCUSSION

Depositional Environment

Organic petrology investigation clearly reveals that the samples are dominated by UOM and liptinite macerals indicating an aquatic, marine environment. The major element data reveal that the lower Cenomanian is rich in silicate minerals and rutile combined with elevated Fe_2O_3 , SiO_2 , Al_2O_3 , K_2O and TiO_2 concentrations indicating more terrigenous input as compared to the overlying, younger units which are carbonate-dominated (Fig. 6). All samples, especially those representing the CTBE are poor in MnO, indicating anoxic bottom water conditions (Calvert and Pedersen, 1993; Aquit *et al.*, 2013). Moreover, phosphorous deposition decreases during increasing anoxic bottom water conditions. Simultaneously the increased availability of phosphorus in the upper water column increases the productivity which further results in declining the

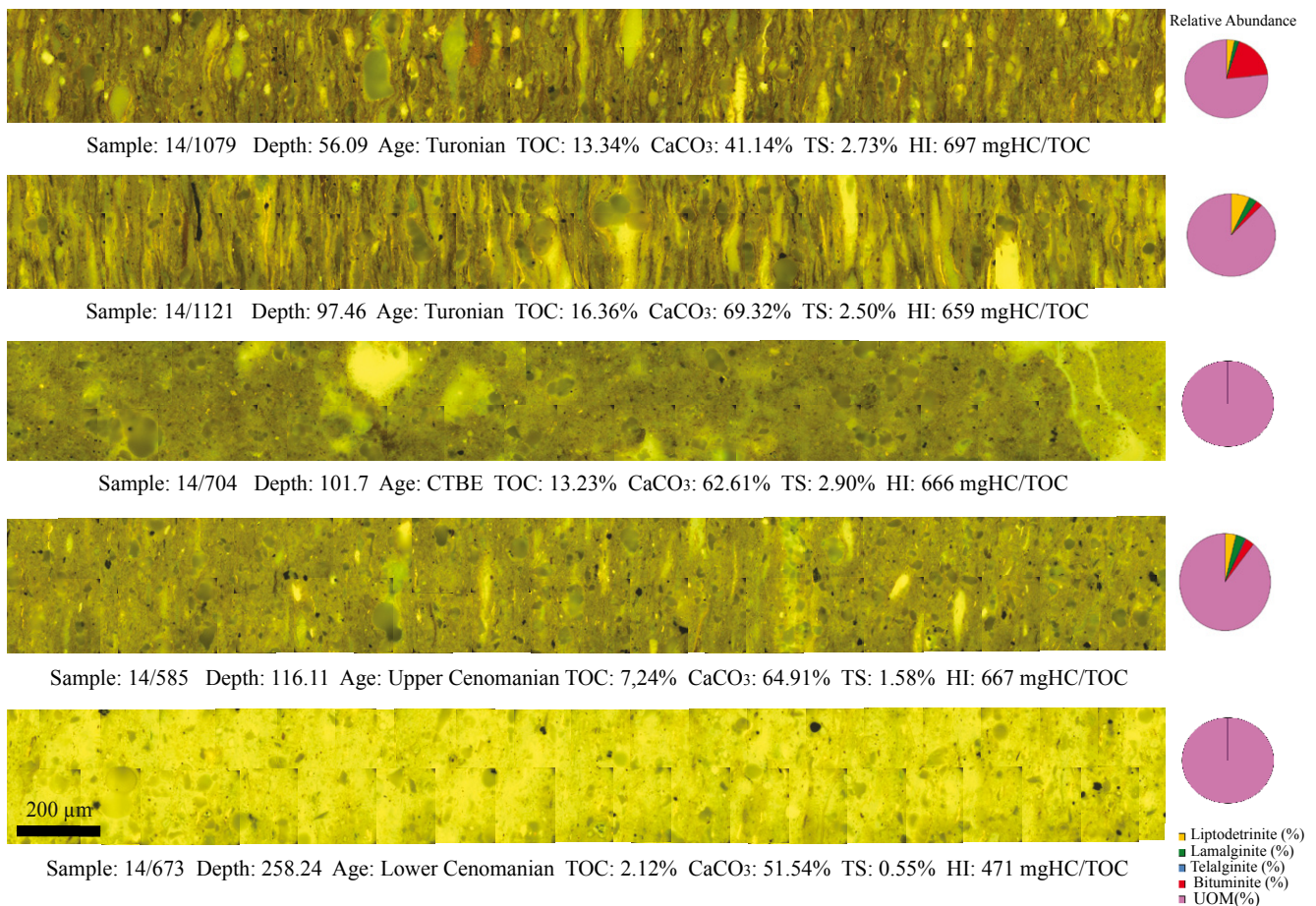


FIGURE 10. Organic matter volume vs. TOC weight percent. The samples that show very low visible organic matter were assigned as 0.2% for the sake of simplicity.

bottom water oxygen (Calvert *et al.*, 1996). Phosphorus usually peaks before the onset of an OAE and retains to its background values after the end of the event (Mort *et al.*, 2007; Jenkyns, 2010). In this well, phosphorus shows elevated values prior to, very low value within and slightly elevated values above the CTBE supporting the previously described hypothesis (Fig. 6). Similar observations of elevated P concentrations were found by Mort (2006) in the Cenomanian of the Mohammed Plage section (Mpl; Fig. 1) and by Nederbragt *et al.* (2004) in the S13 well. Elevated P concentrations prior to the onset of the OAE2 are characteristic of equatorial shelves of the Mid-Cretaceous Proto-Atlantic Ocean as suggested by Kraal *et al.* (2010). These regional data are in accordance with the results in the current study.

Molecular geochemistry data provides excellent environmental indicators. Various different parameters have been used. Pristane (Pr) and phytane (Ph) are two of the most prominent isoprenoids in petroleum samples that originate partly from the phytol side chain of chlorophyll a (Brooks *et al.*, 1969; Powell and McKirdy, 1973; Didyk

et al., 1978). Depending on the oxygen availability the diagenesis of phytol leads either to pristane under more oxic conditions or to phytane under more anoxic conditions (Koopmans *et al.*, 1999; Peters *et al.*, 2005). Therefore, the Pr/Ph ratio has been widely used to characterize the depositional environment (Brooks *et al.*, 1969; Didyk *et al.*, 1978; ten Haven *et al.*, 1987; Powell, 1988). Pr/Ph ratios lower than 1.0 usually indicate anoxic, marine carbonate lithology and values from 1.0 to 1.5 marine shale lithology. Values higher than 2 indicate deltaic shales or terrestrial environments (Peters *et al.*, 2005). Furthermore, the correlation between the Pr/*n*-C₁₇ and Ph/*n*-C₁₈ is used to indicate in more detail kerogen types, depositional environments, thermal maturity and biodegradation (Peters *et al.*, 2005). *n*-Alkane distribution can also be indicative of organic matter input. For example, high abundance of *n*-C₁₅ to *n*-C₂₁ (at low thermal maturity) indicates marine algae and high abundance of *n*-C₂₅-*n*-C₃₁ indicates vascular plant inputs (Yunker *et al.*, 2005).

Using these molecular indicators the following sample characterizations can be deduced. The lower Cenomanian

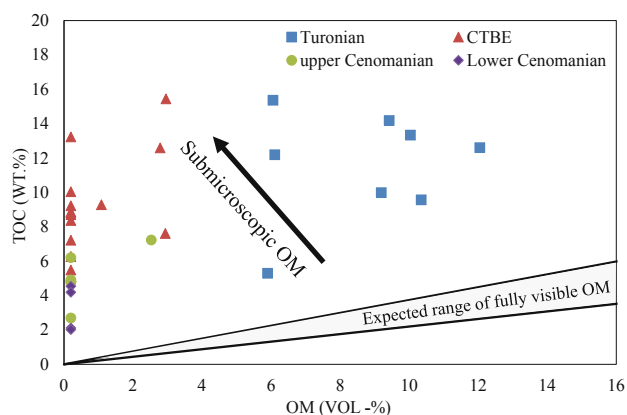


FIGURE 11. Organic matter volume vs. TOC weight percent. The samples that show very low visible organic matter were assigned as 0.2% for the sake of simplicity.

samples show Pr/Ph ~ 1 indicating marine shales and probably more oxic conditions compared to the other samples in this study (Table 2). These samples have a TOC of $\sim 2\%$, HI values of about 500mgHC/TOC and relatively high OI values. Sample 14/653 from the lower/upper Cenomanian boundary shows Pr/Ph lower than 1.0 indicating a change in the depositional environment. All these data suggest that a marine siliclastic depositional environment dominated in the lower Cenomanian, which later shifted to a more carbonate-dominated system. This is in agreement with the elemental data discussed before.

In the upper Cenomanian, Pr/Ph ratios decrease significantly towards the CTBE to descend below 0.32 within it. Higher values occur at the end of the CTBE but remain below 0.8, indicating strong anoxic conditions during the CTBE (Table 2), which support the OAE theory (*i.e.* Jenkyns, 2010; Sachse *et al.*, 2014). The correlation between Pr/ n -C₁₇ and Ph/ n -C₁₈ also indicates the presence of marine organic matter as well as anoxic bottom water conditions (Fig. 12). All samples are also characterized by dominance of n -C₁₆ to n -C₁₉ indicating a major contribution from algae (Cranwell *et al.*, 1987). Pr and Ph occur at higher concentrations than the n -alkanes, which could indicate either biodegradation or very low thermal maturity (Fig. 12). Biodegradation is possible as the samples were taken from relatively shallow depth between 24 and 350m. Furthermore, the geothermal gradient in the Tarfaya Basin is 25°C/km (Zarhloule, 2003) and the average surface temperature is $\sim 19^\circ\text{C}$ implying that the samples are exposed to temperatures of 19 to 27°C. Additionally, the water table in the basin is presently at a depth of approximately 30m (Zarhloule, 2003) and could act as a supplier for nutrients. These conditions favor biodegradation. However, biodegradation is not severe as the n -alkanes are preserved in relatively high abundance and only a small proportion of unresolved complex organic

material was observed (Hedges *et al.*, 2000). Sachse *et al.* (2014) made similar observations of high abundance of Pr and Ph in samples from the younger OAE3 interval in the Tarfaya Basin. Cenomanian and Turonian outcrop samples from the current well vicinity is also similar to the samples in this study, but with more terrigenous characteristics. A reason for this might be the fact that the outcrop samples represent a more proximal area than the samples in this study. Kolonic *et al.* (2002) and Kuypers *et al.* (2004; S13 well) (Fig. 1) briefly discussed the Pr and Ph geochemistry as well and obtained results similar to those of the CTBE samples in this study. Based on their conclusions and in combination with the new results presented in this study, a low thermal maturity is seen as the most probable explanation for the high Pr/ n -C₁₇ and Ph/ n -C₁₈ ratios. An alternative is the contribution of N₂-fixing cyanobacteria that contain chlorophyll a (Ohkouchi *et al.*, 2006; Ricci *et al.*, 2014; see below). The last possible explanation for this phenomenon is that kerogen sulfurization and associated chemical reactions at early diagenesis led to the elevation of phytane and accordingly the pristane

High ratios of steranes to hopanes indicate marine organic matter predominance (Peters *et al.*, 2005). The CTBE samples have sterane/hopane ratios greater than 1.0 indicating dominance of marine algae. This supports the results of the maceral analysis, which show a dominance of alginite, but it should be noted that the major part of the organic matter is submicroscopic.

C₂₇-C₂₉ steranes provide another useful tool to obtain information on the depositional environment and source of kerogen (Fig. 13). High abundance of C₂₈ usually characterizes marine samples (Peters, *et al.*, 2005). Our

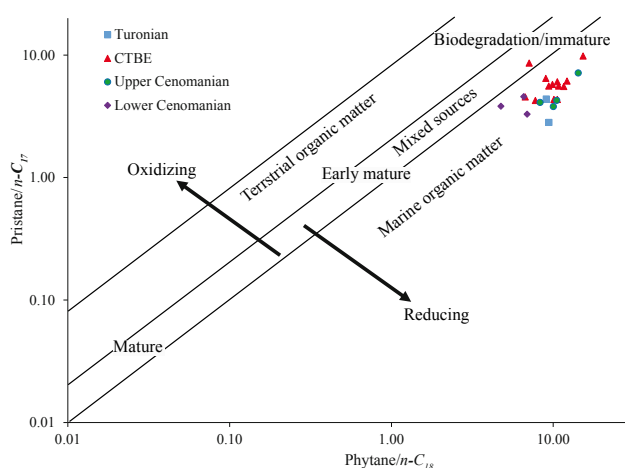


FIGURE 12. Pr/C₁₇ vs. Ph/C₁₈ diagram suggests marine and thermally immature organic matter for all sample. The classification method is from Shanmugam (1985).

TABLE 2. Molecular geochemistry data of the aliphatic fractions

Sample	Depth	Age	Ster/Hop	Pr/Ph	C ₂₈ /C ₂₉ /str	Pr/C ₁₇	Ph/C ₁₈	M-Hop/total Hop
14/1099	75,09	Turonian	1,06	0,36	0,66	2,82	9,40	0,31
14/1119	95,37	Turonian	1,30	0,55	0,54	4,37	9,05	0,29
14/782	100,92	CTBE	0,66	0,71	0,72	6,45	8,99	0,23
14/783	101,67	CTBE	0,90	0,85	0,86	4,55	6,71	0,17
14/784	102,44	CTBE	1,13	0,66	0,90	9,82	15,27	0,18
14/785	103,66	CTBE	1,49	0,88	0,84	8,61	7,10	0,21
14/786	103,97	CTBE	1,61	0,56	0,75	5,54	11,62	0,17
14/787	105,62	CTBE	1,22	0,63	0,97	6,05	10,60	0,25
14/788	106,43	CTBE	1,99	0,45	1,05	6,14	12,16	0,22
14/789	107,64	CTBE	1,70	0,55	0,83	5,75	9,89	0,25
14/790	107,92	CTBE	1,49	0,39	0,85	4,26	7,75	0,21
14/791	109,19	CTBE	1,62	0,37	0,93	5,59	9,39	0,25
14/792	110,48	CTBE	1,26	0,33	0,92	4,34	10,59	0,27
14/794	112,19	CTBE	1,17	0,37	1,06	4,34	10,10	0,26
14/795	113,51	CTBE	1,26	0,34	0,84	5,59	10,80	0,29
14/586	117,03	Upper Cenomanian	1,08	0,46	0,80	4,27	10,51	0,27
14/590	121,18	Upper Cenomanian	1,41	0,45	0,93	3,80	10,00	0,30
14/593	124,05	Upper Cenomanian	1,20	0,54	1,01	7,15	14,26	0,32
14/653	218,74	Upper Cenomanian	1,40	0,77	1,08	4,11	8,29	0,32
14/658	228,07	Lower Cenomanian		0,66	1,19	3,30	6,90	
14/663	238,58	Lower Cenomanian	0,98	1,29	0,90	3,82	4,75	0,35
14/673	258,24	Lower Cenomanian		0,74	1,20	4,57	6,57	

data indicate that the source rocks were deposited in an open to shallow marine/coastal environment and agrees with results from Sachse *et al.* (2011) for outcrop samples from the Cenomanian and Turonian.

Methylated hopanes are used as biomarkers for oxygen-producing and N₂-fixing cyanobacteria and thus the methylated hopanes/hopanes ratio is regarded as a good environmental indicator (Summons *et al.*, 1999; Kuypers *et al.*, 2004b; Peters *et al.*, 2005; Ricci *et al.*, 2014). The cyanobacteria are a diverse group of prokaryotes and contain chlorophyll a, generating oxygen by photosynthesis (Ohkouchi *et al.*, 2006; Ricci *et al.*, 2014). They have no common microscopically identifiable fossils but only molecular ones (Kuypers *et al.*, 2004b). Many of them have the ability to fix N₂ (Ohkouchi *et al.*, 2006). Moreover, Kuypers *et al.* (2004b) and Jenkyns (2010) proposed that cyanobacteria played a major role in the nitrogen cycle and suggested that cyanobacteria were key players during the Cretaceous. Very low methylated hopanes concentrations (<2.0% of total hopanes) typify the samples up to the Jurassic with few exceptions. In contrast, the CTBE samples and the samples from the underlying and overlying Cretaceous units from well SONDAGE-4 show high ratios of methylated hopanes/hopanes indicating concentrations up to 20% (Table 2) which are in line with earlier studies on Cretaceous black shales (Kuypers *et al.*, 2004a).

Translating these ratios into a percentage contribution of cyanobacteria is certainly difficult and only vague. In view of the sterane/hopane ratios (Table 2), n-alkane pattern, and isoprenoid/n-alkane ratios (Fig. 12), and the high HI values of Rock-Eval pyrolysis we can assume that marine phytoplankton was the major contributor to the organic matter, but that both bacteria and cyanobacteria provided additional important pools of the total organic matter, whereas terrigenous contribution was small, which is also supported by microscopic observations (Fig. 10).

Under anoxic depositional environment, sulfate reducing bacteria obtain energy by oxidizing organic compounds and reducing SO₄²⁻ to yield HS⁻¹, HCO₃⁻¹ and remaining non-metabolizable organic matter (Leventhal, 1982; Schulze and Mooney, 1993). These organic residues will constitute the preserved organic carbon in the sediments upon burial (Morse and Berner, 1995). The resulting HS⁻¹ in combination with Fe from pore water or clay will form pyrite (Leventhal, 1982; Berner and Raiswell, 1983; Berner, 1984; Raiswell and Berner, 1986; Dean and Arthur 1989; Schulze and Mooney 1993; Morse and Berner, 1995; Leventhal, 1995). The ratio between the preserved organic carbon and total sulfur (TOC/TS) is used to determine the palaeo-depositional environment (Berner, 1984). Sediments deposited under normal marine conditions (oxic water and typical ocean water salinity)

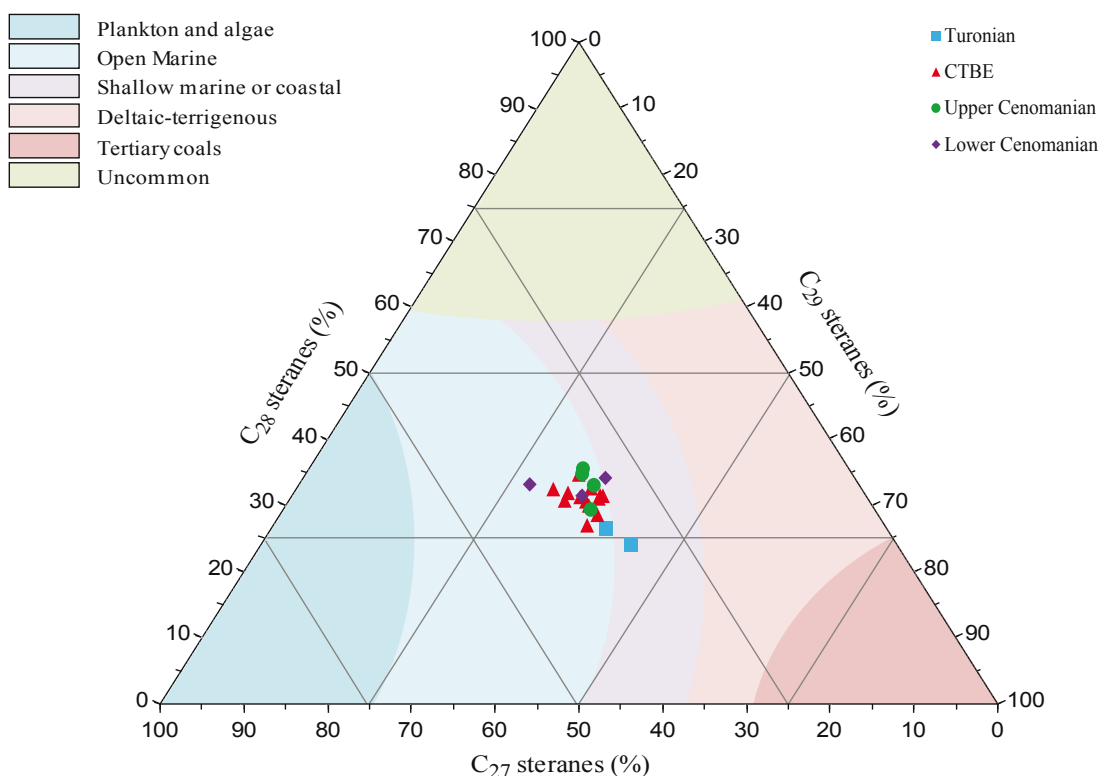


FIGURE 13. C_{27} - C_{29} steranes ternary diagram indicates shallow open marine depositional environment.

will have a TOC/TS ratio of about ~ 2.8 . Higher and lower values characterize lacustrine and euxinic depositional environments, respectively (Berner, 1984), but iron limited carbonate-dominated depositional environments with high organic carbon percentages can also lead to low TOC/TS ratios (Bou Daher *et al.*, 2014, 2015).

However, several factors that control the organic carbon and pyrite formation need to be taken into considerations before using the methods based on Berner (1984). These factors are: i) the presence of metabolizable *versus* non-metabolizable organic matter (type of organic matter), ii) the portion of organic matter that metabolizes through sulfate reduction, iii) the portion of reduced sulfide that is oxidized and not converted to pyrite, iv) the availability and reactivity of reactive detrital iron minerals that react with excess hydrogen sulfide in the system to create pyrite, and v) the sedimentation rate (Leventhal, 1982; Berner and Raiswell, 1983; Berner, 1984; Raiswell and Berner, 1986; Littke *et al.*, 1991; Schulze and Mooney 1993; Canfield, 1994; Leventhal, 1995; Morse and Berner, 1995). In highly calcareous sediments the amount of detrital iron minerals is very limited which results in forming less pyrite than it is expected under normal marine conditions even at high organic carbon contents (Berner, 1984; Raiswell and Berner, 1986; Dean and Arthur, 1989; Bou Daher *et al.*, 2015). Moreover, at high sedimentation rates, the bottom

water oxygen content has negligible influence on organic carbon preservation whereas at low rates only euxinic, oxygen-free bottom water conditions allow for excellent preservation (Canfield, 1994).

In the Tarfaya samples, TS generally correlates positively with TOC (Fig. 14). Most of the samples plot below the normal marine trend line (Berner, 1984) except the samples low in carbonate content, in particular the lower Cenomanian samples. This is similar to other marine, carbonate-rich successions, where the detrital iron supply was limited and thus less pyrite formed (Kolonik *et al.*, 2002; Sachse *et al.*, 2011; Bou Daher *et al.*, 2015).

To further explore the relationship between Fe, TS and TOC, the relationship between sulfur and iron content is displayed in Figure 15. The TS to Fe stoichiometric ratio is 1.15 and plotted as “pyrite line” (Worthmann *et al.*, 1999). The samples of the lower Cenomanian have excess of Fe which holds also true for one of the upper Cenomanian samples (Fig. 15). All younger samples either plot close to the pyrite line or have excess of sulfur indicating the presence of other forms of sulfur such as organic sulfur. This conclusion is supported by the high thiophenes/benzenes ratio derived from the CP-Py-GC-MS data characterizing in particular the CTBE samples (Table 3). All samples from the CTBE show no visible organic matter

TABLE 3. Total thiophenes/total benzenes data from CPPYGCMS data used as a proxy of S_{org}/C_{org}

Sample	Depth (m)	Age	Total thiophenes/ Total benzenes
14/1077	53.52	Turonian	5.54
14/1085	61.40	Turonian	4.35
14/1105	80.08	Turonian	8.18
14/1113	88.70	Turonian	5.12
14/1117	93.20	Turonian	6.26
14/1118	94.45	Turonian	7.06
14/782	100.92	CTBE	5.30
14/705	101.89	CTBE	8.06
14/715	104.02	CTBE	5.35
14/598	129.04	Upper Cenomanian	3.81
14/619	150.23	Upper Cenomanian	3.04
14/628	168.00	Upper Cenomanian	3.69
14/638	187.92	Upper Cenomanian	1.82
14/673	258.24	Lower Cenomanian	3.76
14/678	268.50	Lower Cenomanian	2.21
14/768	305.30	Lower Cenomanian	0.99
14/776	345.05	Lower Cenomanian	0.96

(Fig. 11) possibly indicating that conversion of organic matter into sulfur-bearing kerogen went along with a physical degradation and loss of biogenic morphology of organic particles.

In the process of forming pyrite, 2 moles of organic carbon is required to form one mole of reduced sulfur (Dean and Arthur, 1989; Littke *et al.*, 1991). This means that the original organic carbon content was higher before sulfate reduction, which can be easily deduced from sulfur values *versus* depth profiles within young, marine sediments: at the sediment/water interface, TOC/TS is very high reaching a quite stable value close to 2.8 only at the base of the sulfate reduction zone within the sediments (Littke *et al.*, 1997). In order to obtain the original organic carbon (before sulfate reduction) the following equation was introduced by Littke (1993):

$$TOC_{original} = TOC + 2S * Mc/Ms$$

Where the Mc and Ms are the molecular weight of carbon and sulfur respectively. Subsequently the values of original weight percent of organic matter can be determined using:

$$OM = TOC_{original} * 100/C_{OM}$$

Where C_{OM} is the carbon content of organic matter. Using this value along with the carbonate content we can calculate the silicate content by subtracting the sum of the organic matter and carbonate from 100. Thus the syndimentary system of petroleum source rocks can be represented based on the three major components in a triangular plot (Fig. 16). Limitations of this method are discussed in Littke (1993).

A negative correlation is observed in carbonate-rich samples ($CaCO_3 > 70\%$) between $CaCO_3$ and TOC (Fig. 16; see also Fig. 5), especially for the CTBE and Turonian. This may occur because in a carbonate-dominated environment, enhanced silicate content goes along with enhanced nutrient supply and thus bioproductivity leading to higher organic matter. In contrast, the low-carbonate lower Cenomanian samples show a positive correlation between $CaCO_3$ and TOC, similar to younger, Santonian samples from the Tarfaya Basin (Sachse *et al.*, 2014), indicating that during this episode (lower Cenomanian), nutrient supply was not a limiting factor for organic matter accumulation (see Kuhnt *et al.*, 1997).

Source Rock Potential and Organic Matter Type

Various geochemical techniques were used to evaluate the oil shale and petroleum source rock potential for the samples from the Cenomanian and Turonian, following guidelines on usage of Rock-Eval pyrolysis data by Peters (1986). However, based on Rock-Eval parameters a differentiation between kerogen type II and kerogen type IIS is not possible. Hence, the CP-PY-GC-MS data provide a useful tool to define the kerogen more precisely and to assess the kerogen S_{org}/C_{org} ratio.

The lower Cenomanian samples show very good source rock richness and quality yet the least source rock potential and organic matter quality among the other sections (Figs. 4; 9). In particular, the section between 315.0 and 345m shows very good source rock richness and quality with potential for generating oil at higher maturity. Two samples were analyzed by CP-PY-GC-MS showing low S_{org}/C_{org} ratios. Moreover, the majority of the investigated samples show a lack of bituminite, predominance of UOM associated with alginite and rare vitrinite and inertinite (Fig. 10). This indicates along with the Rock Eval data

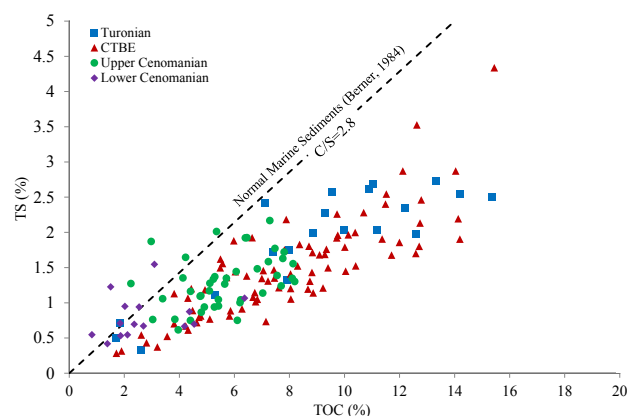


FIGURE 14. TS *versus* TOC cross-plot shows that the majority of the Cenomanian to Turonian samples are plotted below the normal marine line of Berner (1984) unlike the majority of the Lower Cenomanian samples which plot above the line.

that these samples contain kerogen type-II with some of the lower Cenomanian samples containing mixed types II/III (Fig. 8). In addition, the S_{org}/C_{org} are low compared to the younger sections. All maturity parameters suggest that these source rocks are immature.

The upper Cenomanian source rocks have an even greater source rock potential than the lower Cenomanian especially toward the CTBE showing higher TOC and HI values (Figs. 4; 9). With respect to mineralogy, the Cenomanian gently shifts from silicate- to carbonate predominance with highest OM richness occurring when the carbonate content is between 45% and 80% (Fig. 16). The samples evaluated by microscopy show that the majority of the organic matter is unstructured with rarely visible liptinite macerals (Fig. 11). The samples also show a presence of bituminite matrix in fair abundance (Fig. 10C). Pyrolysis data suggest strong presence of thiophenic sulfur compounds compared to the lower Cenomanian indicating the presence of considerable amounts of organic sulfur, *i.e.* kerogen Type IIS. Based on T_{max} and molecular geochemistry these samples are immature.

The Turonian samples are similar to those of the CTBE, but with somewhat lower S_{org} . They also differ from the CTBE in organic matter type especially in the younger interval (Turonian), where a high amount of bituminite is observed as well as alginite (Fig. 10A).

Oil generation potential of the entire sequence is very high, with a tendency of sulfur-rich oil being generated especially within the CTBE. Sulfur-rich kerogen is known to generate first petroleum at lower temperatures than sulfur-poor kerogen (Pepper and Corvi, 1995).

In comparison with literature data compiled in Wenke (2014) for the on-offshore Tarfaya Basin, the sample set supports the excellent source rock potential of the Late Cretaceous. Increasing amounts of OM were measured in the onshore area, whilst very high amounts have not been reported for the offshore area (Wenke, 2014). TOC values average 3% and HI values of 140-400mgHC/g rock were published (Wenke, 2014). Moderate-high values of 0.8 to 4% TOC were measured on the shelf (HI 150-400mgHC/g rock), and up to 6% on the slope (Wenke, 2014).

The CTBE source rocks are globally distributed and studied in great detail in North Africa and Mid-Atlantic regions (*e.g.* Herbin *et al.*, 1986; Schlanger *et al.*, 1987; Foster *et al.*, 2004; Lüning *et al.*, 2004; Jenkyns, 2010). All of the above mentioned studied locations exhibited high TOC values within wide ranges based on the depositional environmental conditions. Limited information is available on the kerogen sulfurization during the CTBE, but TS enrichments were recorded widely during this time.

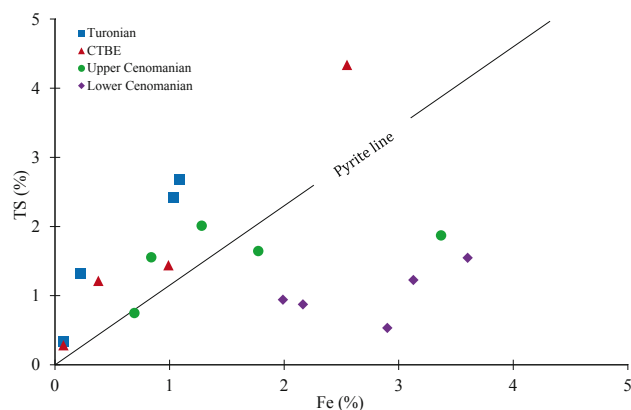


FIGURE 15. TS versus Fe shows that the majority of the samples from Cenomanian to Turonian are plotted above the Pyrite line indicating that the sulfur in these samples is present in other forms than pyrite.

Two Albian samples show an excellent source rock potential (Table I). Due to the low number of samples only Rock Eval and TOC analyses were conducted with no further geochemical investigation. Nevertheless, the available data support the general idea of an Albian source rock in the Tarfaya Basin. Wenke (2014) related the increasing source rock potential during the Albian to the termination of the TanTan Delta. This also matches with results of Sachse *et al.* (2011), who identified the Albian source rock further onshore as being only of marginal quality (low TOC and HI). Thus, a high variation of organic matter quantity and quality based on the spatial and temporal distribution of the Albian deposits can be assumed.

Kerogen Diagenesis and Properties

The formation and preservation of kerogen results from two main pathways which are: i) the selective preservation

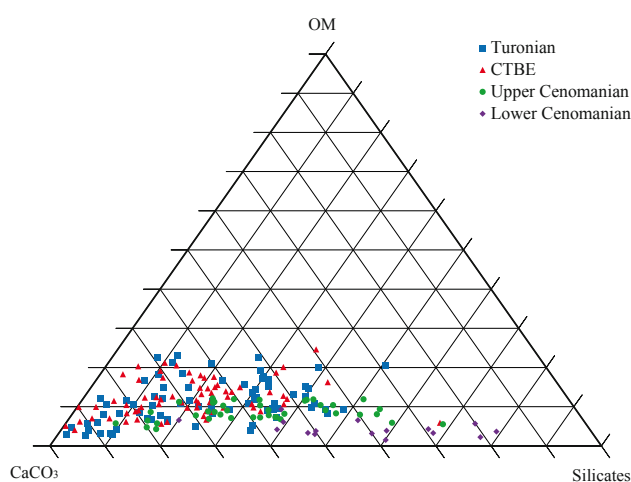


FIGURE 16. OM-CaCO₃-Silicates ternary diagram (modified after Littke, 1993) showing that the best organic preservation is achieved at CaCO₃ concentration between 45 to 80%.

and ii) degradation-recondensation pathways (Largeau and Derenne, 1993). The first pathway is based on the existence of the insoluble and non-hydrolysable macromolecules in the outer walls of the original species (Derenne *et al.*, 1992) that is resistant to microbial and chemical alteration at the diagenesis stage. The second pathway for kerogen formation is a complete restructuring of the organic matter due to degradation followed by recondensation (Welte, 1972; Tissot and Welte, 1984; Largeau and Derenne, 1993; Taylor *et al.*, 1998). The lack of resistant macromolecules will result in the formation of the unstructured organic matter (UOM) (Largeau and Derenne, 1993).

One essential mechanism destroying the morphology of organic matter is the early diagenetic vulcanization process which is related to sulfur incorporation into the organic matter (Taylor *et al.*, 1998). Moreover, cyanobacteria through selective preservation pathway could result in UOM (Pacton *et al.*, 2006). The samples from the upper Turonian to Cenomanian show high S_{org}/C_{org} values and high proportions of amorphous kerogen with extreme abundance in the samples representing the CTBE. These samples have high S_{org}/C_{org} values and lower amorphous kerogen abundance in the upper section, indicating early diagenetic reactions between sulfur and organic matter. De Leeuw and Sinninghe-Damsté (1990) showed that reaction between H_2S or HS_x^- with phytol esters or phytol will result in thiol which will react with the functionalities of other compounds to produce larger materials. This process saves phytol precursors from degradation in the upper part of the sediments. With increasing diagenesis the C-S bonds are cleaved and phytane is generated after hydrogenation of intermediate phytanes and phytadienes.

Littke and Sachsenhofer (1994) showed that source rocks from upwelling areas are generally characterized by dominance of UOM associated with small particles of alginite and rare terrestrial organic matter. This hypothesis fits perfectly the studied samples which are clearly dominated by submicroscopic organic matter.

CONCLUSIONS

Rock-Eval and elemental analysis results reveal excellent source rock potential for the entire, thick lower Cenomanian to Turonian section. Based on Rock-Eval evaluation, there are two main groups of source rocks which are i) moderately high in TOC and HI, comprising the lower Cenomanian and ii) high in TOC and HI from the upper Cenomanian to Turonian.

Organic matter characterization based on molecular geochemistry shows a marine origin for the organic matter in the Cenomanian to Turonian samples. This is supported

by microscopic analysis that suggested predominance of UOM associated with alginite and rare vitrinite and inertinite. The samples show different levels of kerogen sulfurization depending on the depositional environment. Therefore, the samples are classified based on the organic sulfur content as i) S_{org} -rich ($S_{org}/C_{org} = 5-8$), *i.e.* the CTBE and Turonian samples, ii) S_{org} -moderately rich ($S_{org}/C_{org} \sim 3.5$), *i.e.* the Upper Cenomanian and iii) S_{org} -poor ($S_{org}/C_{org} < 1$), *i.e.* the lower Cenomanian.

The upper Cenomanian to Turonian are characterized by relatively high carbonate content and the samples from the lower Cenomanian are characterized by high silicate content. The highest organic matter content is found when the carbonate content is between 50 to 80 %. All samples were deposited under anoxic conditions with the highest oxygen depletion occurring during the CTBE based on biomarker data, coupled with high sea water temperatures. Samples younger than the silicate-rich lower Cenomanian interval are expected to generate sulfur-rich oil.

In conclusion, the integrated study elucidates possible processes leading to the source rock development and kerogen formation within the Cenomanian and Turonian section. Furthermore, it supports the idea of an Albian source rock potential in the Tarfaya Basin, which seems, however, relatively local. The study investigated the relative organic sulfur enrichment which is of great importance, *e.g.* for the oil shale retorting. Further quantitative analyses are highly recommended on this aspect.

ACKNOWLEDGMENTS

The authors want to thank ALAGO (Latin American Association of Organic Geochemistry) for the invitation to publish in this special volume. The authors would like to thank the marine micropaleontology group at Kiel University for providing the samples and biostratigraphic data, especially Dr. Wolfgang Kuhnt, Dr. Ann Holbourn and Dr. Mohamed Aquit. The first author would like to thank Saudi Aramco for funding the project as part of his PhD program. Special thanks also to Diana Marcela Chaves Saldana and Jan Gronewald for their great help in the lab work and to Alexander Stock for helping in the sampling. We thank Dr. Albert Permanyer and an anonymous reviewer for their constructive comments on an earlier draft of this manuscript.

REFERENCES

- Aquit, M., Kuhnt, W., Holbourn, A., Chellai, E., Statterger, K., Kluth, O., Jabour, H., 2013. Late Cretaceous paleoenvironmental evolution of the Tarfaya Atlantic coastal Basin, SW Morocco. *Cretaceous Research*, 45, 288-305.

- Berner, R.A., 1984. Sedimentary pyrite formation: an update. *Geochimica et Cosmochimica Acta*, 48, 605-615.
- Berner, R.A., Raiswell, R., 1983. Burial of organic carbon and pyrite sulfur in sediments over Phanerozoic time: a new theory. *Geochimica et Cosmochimica Acta*, 47, 855-862.
- Bou Daher, S., Nader, F.H., Strauss, H., Littke, R., 2014. Depositional environment and source-rock characterization of organic-matter rich upper Santonian – upper Campanian carbonates, Northern Lebanon. *Journal of Petroleum Geology*, 37, 5-24
- Bou Daher, S., Nader, F.H., Müller, C., Littke, R., 2015. Geochemical and petrographic characterization of Campanian – Lower Maastrichtian calcareous petroleum source rocks of Hasbaya, South Lebanon. *Marine and Petroleum Geology*, 64, 304-323
- Brooks, J.D., Gould, K., Smith, J.W., 1969. Isoprenoid hydrocarbons in coal and petroleum. *Nature*, 222, 257-259.
- Calvert, S.E., Pedersen, T.F., 1993. Geochemistry of Recent oxic and anoxic marine sediments: Implications for the geological record. *Marine Geology*, 113(1-2), 67-88.
- Calvert, S.E., Bustin, R.M., Ingall, E.D., 1996. Influence of water column anoxia and sediment supply on the burial and preservation of organic carbon in marine shales. *Geochimica et Cosmochimica Acta*, 60(9), 1577-1593.
- Canfield, D.E., 1994. Factors influencing organic carbon preservation in marine sediments. *Chemical Geology*, 114, 315-329.
- Cranwell, P.A., Eglinton, G., Robinson, N., 1987. Lipids of aquatic organisms as potential contributors to lacustrine sediments-II. *Organic Geochemistry*, 11(6), 513-527.
- Creaney, S., 1980. Petrographic texture and vitrinite reflectance variation on the alston block, north-east England. *Yorkshire Geological Society*, 42(4), 553-580.
- Davison, I., 2005. Central Atlantic margin basins of North West Africa: Geology and hydrocarbon potential (Morocco to Guinea). *Journal of African Earth Sciences*, 43, 254-274.
- de Leeuw J.W., Sinninghe-Damsté J.S., 1990. Organic sulphur compounds and other biomarkers as indicators of paleosalinity. In: Orr, W.L., White, C.M. (eds.). *Geochemistry of Sulfur in Fossil Fuels*. American Chemical Society 1st edition. 417-443.
- Dean, W.E., Arthur, M.A., 1989. Iron-sulfur-carbon relationships in organic-carbon-rich sequences: I. Cretaceous Western Interior Seaway. *American Journal of Science*. 289, 708-743.
- Derenne, S., Largeau, C., Berkaloﬀ, C., Rousseau, B., Wilhelm, C., Hatcher, P.G., 1992. Non-hydrolysable macromolecular constituents from outer walls of *Chlorella fusca* and *Nanochlorum eucaryotum*. *Phytochemistry*, 31, 1923-1929.
- Didyk, B.M., Simoneit, B.R.T., Brassell, S.C., Eglinton, G., 1978. Organic geochemical indicators of palaeoenvironmental conditions of sedimentation. *Nature*, 272, 216-222.
- Dyni, J.R., 2006. Geology and resources of some world oil-shale deposits. U.S. Geological Survey Scientific Investigations Report, 2005-5294, 42pp.
- Einsele, G., Wiedmann, J., 1982. Turonian Black Shales in the Moroccan Coastal Basins: First Upwelling in the Atlantic Ocean? In: Von Rad, U., Hinz, K., Sarnthein, M., Seibold, E. (eds.). *Geology of the Northwest African Continental Margin*. Springer Berlin Heidelberg, 396-414.
- Enachescu, M.E., Hogg, J.R., Fowler, M., Brown, D.E., Atkinson, I., 2010. Late Jurassic Source Rock Super-Highway on Conjugate Margins of the North and Central Atlantic (offshore East Coast Canada, Ireland, Portugal, Spain and Morocco). Central and North Atlantic Conjugate Margins conference, Lisbon 2010. Volume II, 49-80. ISBN: 978-989-96923-0-5
- Erbacher, J., Thurow, J., Littke, R., 1996. Evolution patterns of radiolaria and organic matter variations: A new approach to identify sea-level changes in Mid-Cretaceous pelagic environments. *Geology*, 24, 499-502.
- Espitalié, J., Deroo, G., Marquis, F., 1985. La pyrolyse Rock-Eval et ses applications. *Revue de l'Institut Français du Pétrole*, 40, 563-579.
- Hafid, M., Tari, G., Bouhadioui, B., El Moussaid, I., Echcharfaoui, H., Ait Salem, A., Nahim, M., Dakki, M., 2008. Atlantic basins. In: Michard, A., Saddiqi, O., Chalouan, A., Frizon de Lamotte, D. (eds.). *Continental evolution: The Geology of Morocco*. Lecture Notes in Earth Sciences, 116, 303-329.
- ten Haven, H.L., de Leeuw, J.W., Rullkötter, J., Sinninghe Damsté, J.S., 1987. Restricted utility of the pristane/phytane ratio as a paleoenvironmental indicator. *Nature*, 330, 641-643.
- Hedges, J.I., Eglinton, G., Hatcher, P.G., Kirchman, D.L., Arnosti, C., Derenne, S., Evershed, R.P., Kögel-Knabner, I., de Leeuw, J.W., Littke, R., Michaelis, W., Rullkötter, J., 2000. The molecularly-uncharacterized component of nonliving organic matter in natural environments. *Organic Geochemistry*, 31(10), 945-958.
- Herbin, J.P., Montadert, L., Müller, C., Gomez, R., Thurow, J., Wiedmann, J., 1986. Organic-rich sedimentation at the Cenomanian-Turonian boundary in oceanic and coastal basins in the North Atlantic and Tethys. *London, Geological Society*, 21(1, Special Publications), 389-422.
- Hutton, A.C., 1987. Petrographic classification of oil shales. *International Journal of Coal Geology*, 8, 203-231.
- Jenkyns, H.C., 1980. Cretaceous anoxic events: from continents to oceans. *London, Journal of Geological Society*, 137, 171-188.
- Jenkyns, H.C., 2010. Geochemistry of oceanic anoxic events. *Geochemistry Geophysics Geosystems*, 11(3), Q03004. DOI:10.1029/2009GC002788
- Kolonis, S., Sinninghe Damsté, J.S., Bottcher, M.E., Kuypers, M.M.M., Kuhnt, W., Beckmann, B., Scheeder, G., Wagner, T., 2002. Geochemical Characterization of Cenomanian/Turonian Black Shales from the Tarfaya Basin (SW Morocco). *Journal of Petroleum Geology*, 25, 325-350.
- Koopmans, M.P., Irene; W., Rijpstra, C., Klapwijk, M.M., de Leeuw, J.W., Lewan, M.D., Damsté, J.S.S., 1999. A thermal and chemical degradation approach to decipher pristane and phytane precursors in sedimentary organic matter. *Organic Geochemistry*, 30, 1089-1104.
- Kraal, P., Slomp, C.P., Forster, A., Kuypers, M.M., 2010. Phosphorus cycling from the margin to abyssal depths

- in the proto-Atlantic during oceanic anoxic event 2. *Palaeogeography, Palaeoclimatology, Palaeoecology*, 295(1), 42-54.
- van Krevelen, D.W., 1950. Graphical-statistical method for the study of structure and reaction processes of coal. *Fuel*, 29, 269-84.
- Kuhnt, W., Nederbragt, A., Leine, L., 1997. Cyclicity of Cenomanian-Turonian organic-carbon-rich sediments in the Tarfaya Atlantic Coastal Basin (Morocco). *Cretaceous Research*, 18, 587-601.
- Kuhnt, W., Holbourn, A., Gale, A., Chellai, E.A., Kennedy, J., 2009. Cenomanian sequence stratigraphy and sea-level fluctuations in the Tarfaya Basin (SW Morocco). *Geological Society America Bulletin*, 121, 1695-1710.
- Kuypers, M.M.M., van Breugel, Y., Schouten, S., Erba, E., Sinninghe Damsté, J.S., 2004b. N₂-fixing cyanobacteria supplied nutrient N for Cretaceous oceanic anoxic events. *Geology*, 32(10), 853-856.
- Kuypers, M.M.M., Lourens, L.J., Rijpstra, W., Pancost, R., Nijenhuis, I.A., Sinninghe Damsté, J.S., 2004a. Orbital forcing of organic carbon burial in the proto-North Atlantic during oceanic anoxic event 2. *Earth and Planetary Science Letters*, 228, 465-482.
- Lancelot, Y., Winterer, E.L., 1980. Evolution of the Moroccan oceanic basin and adjacent continental margin; a synthesis. United States, Initial Reports of the Deep Sea Drilling Project 50 Publisher: Texas A & M University, Ocean Drilling Program, College Station, 801-821.
- Largeau, C., Derenne, S., 1993. Relative efficiency of the selective preservation and degradation recondensation pathways in kerogen formation. Source and environment influence on their contributions to type I and II kerogens. *Organic Geochemistry*, 20, 611-616.
- Leventhal, J.S., 1982. An interpretation of carbon and sulfur relationships in Black Sea sediments as indicators of environments of deposition. *Geochimica et Cosmochimica Acta*, 47, 133-137.
- Leventhal, J.S., 1995. Carbon-sulfur plots to show diagenetic and epigenetic sulfidation in sediments. *Geochimica et Cosmochimica Acta*, 59, 1207-1211.
- Littke, R., 1993. Deposition, Diagenesis and Weathering of Organic Matter-Rich Sediments. Lecture Notes in Earth Sciences, Berlin, Springer Verlag, 216pp.
- Littke, R., Sachsenhofer, R.F., 1994. Organic petrology of deep sea sediments: a compilation of results from the Ocean Drilling Program and the Deep Sea Drilling Project. *Energy and Fuels*, 8, 1498-1512.
- Littke, R., Baker, D.R., Leythaeuser, D., Rullkötter, J., 1991. Keys to the depositional history of the Posidonia Shale (Toarcian) in the Hils syncline, Northern Germany. In: Tyson, R.V., Pearson, T. (eds.). *Modern and ancient continental shelf anoxia*. Geological Society, 58 (Special publications), 311-334.
- Littke, R., Lückge, A., Welte, D.H., 1997. Quantification of organic matter degradation by microbial sulphate reduction for Quaternary sediments from the northern Arabian Sea. *Naturwissenschaften*, 84, 312-315.
- Lüning, S., Kolonic, S., Belhadj, E.M., Belhadj, Z., Cota, L., Baric, G., Wagner, T., 2004. Integrated depositional model for the Cenomanian-Turonian organic-rich strata in North Africa. *Earth-Science Reviews*, 64, 51-117.
- Michard, A., Saddiqi, O., Chalouan, A., Frizon de Lamotte, D. (eds.), 2008. *Continental Evolution: The Geology of Morocco. Structure, Stratigraphy, and Tectonics of the Africa-Atlantic-Mediterranean Triple Junction*. Lecture Notes in Earth Sciences, Berlin, Heidelberg, Springer-Verlag, 424pp.
- Morabet, A.M., Bouchta, R., Jabour, H., 1998. An overview of the petroleum systems of Morocco. In: Mac-Gregor, D.S., Moody, R.T.J., Clark-Lowes, D.D. (eds.). *Petroleum Geology of North Africa*. London, Geological Society, 132 (Special Publications), 283-296.
- Morse, J.W., Berner, R.A., 1995. What determines sedimentary C/S ratios? *Geochimica et Cosmochimica Acta*, 59, 1073-1077.
- Mort, H., 2006. Biogeochemical changes during the Cenomanian-Turonian Oceanic Anoxic Event (OAE 2). Doctoral dissertation. Université de Neuchâtel. 205.
- Mort, H.P., Adatte, T., Föllmi, K.B., Keller, G., Steinmann, P., Matera, V., Berner, Z., Stüben, D., 2007. Phosphorus and the roles of productivity and nutrient recycling during oceanic anoxic event 2. *Geology*, 35, 483-486.
- Mort, H.P., Adatte, T., Keller, G., Bartels, D., Föllmi, K.B., Steinmann, P., Berner, Z., Chellai, E.H., 2008. Organic carbon deposition and phosphorus accumulation during Oceanic Anoxic Event 2 in Tarfaya, Morocco. *Cretaceous Research*, 29(5-6), 1008-1023. ISSN: 0195-6671
- Nederbragt, A.J., Thurow, J., Vonhof, H., Brumsack, H.J., 2004. Modelling oceanic carbon and phosphorus fluxes: implications for the cause of the late Cenomanian Oceanic Anoxic Event 2 (OAE2). *Journal of the Geological Society*, 161, 721-728.
- Neumaier, M., Back, S., Littke, R., Kukla, P.A., Schnabel, M., Reichert, C., 2015. Late Cretaceous to Cenozoic geodynamic evolution of the Atlantic margin offshore Essaouira (Morocco). *Basin Research*, 1-19. DOI: 10.1111/bre.12127
- Ohkouchi, N., Kashiyama, Y., Kuroda, J., Ogawa, N.O., Kitazato, H., 2006. The importance of diazotrophic cyanobacteria as a primary producers during Cretaceous Oceanic Anoxic Event 2. *Biogeosciences*, 3, 575-605.
- Pacton, M., Fiet, N., Gorin, G., 2006. Revisiting amorphous organic matter in Kimmeridgian laminites: what is the role of the vulcanization process in the amorphization of organic matter? *Terra Nova*, 18, 380-387.
- Pepper, A.S., Corvi, P.J., 1995. Simple kinetic models of petroleum formation. Part I: oil and gas generation from kerogen. *Marine and Petroleum Geology*, 12(3), 291-319. ISSN 0264-8172
- Peters, K.E., 1986. Guidelines for evaluating petroleum source rock using programmed pyrolysis. *American Association of Petroleum Geologists Bulletin*, 70, 318-329.

- Peters, K.E., Walters, C.C., Moldowan, J.M., 2005. The Biomarker Guide, Volume 2. Biomarkers and Isotopes in Petroleum Exploration and Earth History. Cambridge, Cambridge University Press, 2nd edition, 1155.
- Powell, T.G., 1987. Pristane/phytane ratio as environmental indicator. *Nature*, 333, 604.
- Powell, T.G., McKirdy, D.M., 1973. Relationship between ratio of pristane to phytane, crude oil composition and geological environment in Australia. *Nature*, 243, 37-39.
- Raiswell, R., Berner, R.A., 1986. Pyrite and organic-matter in Phanerozoic normal marine shales. *Geochimica et Cosmochimica Acta*, 50(9), 1967-1976.
- Ricci, J.N., Coleman, M.L., Welander, P.V., Sessions, A.L., Summons, R.E., Spear, J.R., Newman, D.K., 2014. Diverse capacity for 2-methylhopanoid production correlates with a specific ecological niche. *International Society for Microbial Ecology. Journal*, 8, 675-684. DOI:10.1038/ismej.2013.191
- Ricken, W. 1993. Sedimentation as a three-component system. *Lecture Notes in Earth Sciences*, 51, 1- 211.
- Saadi, M., Hital, E.A., Bensaïd, M., Boudda, A., Dahmani, M., 1985. Carte Géologique du Maroc. Éditions du Service Géologique du Maroc- Notes et Mémoires, 260.
- Sachse, V.F., Littke, R., Heim, S., Kluth, O., Schober, J., Boutib, L., Jabour, H., Perssen, F., Sintern, S., 2011. Petroleum source rocks of the Tarfaya Basin and adjacent areas, Morocco. *Organic Geochemistry*, 42, 209-227.
- Sachse, V.F., Littke, R., Jabour, H., Schumann, T., Kluth, O., 2012. Late Cretaceous (Late Turonian, Coniacian and Santonian) petroleum source rocks as part of an OAE, Tarfaya Basin, Morocco. *Marine and Petroleum Geology*, 29, 35-49.
- Sachse, V.F., Heim, S., Jabour, H., Kluth, O., Schumann, T., Aquit, M., Littke, R., 2014. Organic geochemical characterization of Santonian to Early Campanian organic matter-rich marls (Sondage No 1 cores) as related to OAE3 from the Tarfaya Basin, Morocco. *Marine and Petroleum Geology*, 56, 290-304.
- Schlanger, S.O., Jenkyns, H.C., 1976. Cretaceous anoxic events: Causes and consequences. *Geologie en Mijnbouw*, 55, 179-184.
- Schlanger, S.O., Arthur, M.A., Jenkyns, H.C., Scholle, P.A., 1987. The Cenomanian-Turonian Oceanic Anoxic Event, I. Stratigraphy and distribution of organic carbon-rich beds and the marine $\delta_{13}\text{C}$ excursion. London. Geological Society, 26(1), Special Publication, 371-399.
- Schönfeld, J., Kuhnt, W., Erdem, Z., Flögel, S., Glock, N., Aquit, M., Frank, M., Holbourn, A., 2015. Records of past mid-depth ventilation: Cretaceous ocean anoxic event 2 vs. Recent oxygen minimum zones. *Biogeosciences*, 12(4), 1169-1189.
- Schulze, E., Mooney, H.A., 1993. Biodiversity and ecosystem function. Berlin, Springer-Verlag, 521pp.
- Schwarzbauer, J., Littke, R., Weigelt, V., 2000. Identification of specific organic contaminants for estimating the contribution of the Elbe river to the pollution of the German Bight. *Organic Geochemistry*, 31, 1713-1731.
- Senftle, J.T., Landis, C.R., McLaughlin, R.L., 1993. Organic petrographic approach to kerogen characterisation. In: Engel, M.H., Macko, S.A. (eds.). *Organic Geochemistry. Principles and Applications*. New York, Plenum Press, 355-374.
- Shanmungam, G., 1985. Significance of coniferous rain forests and related organic matter in generating commercial quantities of oil, Gippsland Basin, Australia. *The American Association of Petroleum Geologists Bulletin*, 69, 1241-1254.
- SubsealQ, 2014. Website: http://www.subseaiq.com/data/Project.aspx?project_id=1742#history. last accessed in 12 November 2016.
- Summons, R.E., Jahnke, L.L., Hope, J.M., Logan, G.A., 1999. 2-Methylhopanoids as biomarkers for cyanobacterial oxygenic photosynthesis. *Nature*, 400, 554-57
- Taylor, G.H., Teichmüller, M., Davis, A., Diessel, C.F.K., Littke, R., Robert, P., 1998. *Organic Petrology*. Stuttgart, Borntraeger, 704pp.
- Teichmüller, M., Ottenjann, K., 1977. Art und Diagenese von Liptiniten und lipoiden Stoffen in einem Erdölmuttergestein auf Grund fluoreszenzmikroskopischer Untersuchungen. *Erdöl und Kohle*, 30, 387-398.
- Tissot, B., Welte, D.H., 1984. *Petroleum Formation and Occurrence*. New York, Springer- Verlag, 699pp.
- Welte, D.H., 1972. Petroleum exploration and organic geochemistry. *Journal of Geochemical Exploration*, 1, 117-136.
- Wenke, A.A.O., 2014. Sequence stratigraphy and basin analysis of the Meso- to Cenozoic Tarfaya-Laâyoune. Basins, on- and offshore Morocco. Doctoral Thesis. Heidelberg, Ruprecht-Karls-Universität, 191pp. URN:nbn:de:bsz:16-heidok-179058
- Wenke, A.A.O., Zühlke, R., Jabour, H., Kluth, O., 2011. High-resolution sequence stratigraphy in basin reconnaissance: example from the Tarfaya Basin, Morocco. *First break*, 29, 85-96.
- Worthmann, U.G., Hesse, R., Zacher, W., 1999. Major-element analysis of cyclic black shales: paleoceanographic implications for the Early Cretaceous deep western Tethys. *Paleoceanography*, 14, 525-541.
- Yunker, M.B., Belicka, L.L., Harvey, H.R., Macdonald, R.W., 2005. Tracing the inputs and fate of marine and terrigenous organic matter in Arctic Ocean sediments: A multivariate analysis of lipid biomarkers. *Deep-Sea Research II*, 52, 3478-3508.
- Zarhloule, Y., 2003. Overview of Geothermal Activities in Morocco. *Proceedings of the International Geothermal Conference 2003*, S10, P9.

Manuscript received September 2015;
revision accepted May 2016;
published Online November 2016.

APPENDIX I

TABLE I. Elemental and Rock Eval 6 data. Units: *mgHC/Rock, **mgCO₂/gRock, ***mgHC/gTOC, ****mgCO₂/gTOC. T: Turonian, CT: CTBE, UC: Upper Cenomanian, LC: Lower Cenomanian A: Albian

Sample	Depth [m]	Age	TOC (%)	CaCO ₃ (%)	S (%)	TS/TOC	Original OM (%)	Silicates (%)	S1 *	S2 *	S3 **	Tmax (°C)	HI ***	OI ****
14/1047	24.06	T	5.56	78.75										
14/1048	24.7	T	4.77	88.25										
14/1049	26.22	T	6.50	66.32										
14/1050	26.56	T	9.02	68.82										
14/1051	27.67	T	6.39	83.31										
14/1052	28.6	T	5.30	86.16	1.11	0.21	8.03	5.81	0.73	39.48	1.55	411	745	29
14/1053	29.66	T	8.45	46.53										
14/1054	30.7	T	7.22	45.36										
14/1055	31.61	T	8.45	70.85										
14/1056	32.5	T	8.07	76.18										
14/1057	33.42	T	5.62	55.22										
14/1058	34.6	T	7.32	62.80										
14/1059	35.52	T	7.89	67.89										
14/1060	36.81	T	10.68	56.48										
14/1061	37.61	T	9.75	56.29										
14/1062	38.57	T	2.19	95.66										
14/1063	39.71	T	8.18	79.60										
14/1064	40.47	T	2.31	87.07										
14/1065	41.38	T	1.69	92.22	0.49	0.29	2.72	5.06	0.10	13.36	1.34	409	790	79
14/1066	42.57	T	5.28	78.25										
14/1067	43.6	T	8.54	58.47										
14/1068	44.75	T	2.49	89.25										
14/1069	45.53	T	14.19	60.24	2.55	0.18	21.05	18.71	2.72	95.56	3.39	412	673	24
14/1070	46.62	T	4.14	60.59										
14/1071	47.63	T	4.89	75.56										
14/1072	48.63	T	6.00	76.16										
14/1073	49.6	T	10.89	51.98	2.62	0.24	16.89	31.13	1.81	81.34	3.36	410	747	31
14/1074	50.68	T	7.23	54.76										
14/1075	51.69	T	8.44	53.80										
14/1076	52.8	T	8.49	46.51										
14/1077	53.52	T	7.13	56.91	2.41	0.34	11.84	31.24	1.01	48.75	1.65	412	684	23
14/1078	54.73	T	9.84	47.31										
14/1079	56.09	T	13.34	41.14	2.73	0.20	20.16	38.70	2.25	92.94	3.48	410	697	26
14/1080	57.07	T	11.54	45.65										
14/1081	57.5	T	8.00	73.37	1.75	0.22	12.22	14.41	0.89	54.43	1.61	414	680	20
14/1082	58.04	T	7.92	65.57					1.19	51.92	1.59	413	656	20
14/1083	59.15	T	7.10	56.08					0.92	48.44	1.55	408	682	22
14/1084	60.23	T	3.05	61.71					0.25	20.70	1.58	410	679	52
14/1085	61.4	T	1.85	87.42	0.72	0.39	3.17	9.41	0.14	14.66	1.28	410	792	69
14/1086	62.05	T	7.18	42.18					0.98	50.79	1.49	413	709	21
14/1087	62.86	T	6.40	45.60					0.62	42.40	1.64	413	662	26
14/1088	64.07	T	3.07	91.07					0.41	23.05	1.65	409	751	54
14/1089	65.02	T	9.99	52.79	2.03	0.20	15.08	32.13	1.30	72.51	3.17	410	726	32
14/1090	66.125	T	11.65	67.31										
14/1091	67.105	T	3.79	71.19										
14/1092	68.13	T	5.27	75.29										
14/1093	69.04	T	7.42	64.85	1.72	0.23	11.43	23.72	1.06	51.66	1.56	412	696	21
14/1094	70.14	T	7.54	53.97										
14/1095	71.02	T	7.55	54.75										
14/1096	72.1	T	10.24	49.25										
14/1097	73.24	T	9.28	55.47	2.28	0.25	14.45	30.08	1.33	70.10	2.99	410	755	32
14/1098	74.06	T	7.58	47.74										
14/1099	75.09	T	9.57	46.09	2.58	0.27	15.15	38.75	1.17	70.79	3.05	410	740	32
14/1100	76.32	T	13.81	52.39										
14/1101	77.11	T	8.87	56.45	1.98	0.22	13.60	29.95	1.23	71.49	3.05	410	806	34
14/1102	78.31	T	3.34	85.79										
14/1103	79.27	T	14.92	52.26										

TABLE I. (Cont.)

Sample	Depth [m]	Age	TOC (%)	CaCO ₃ (%)	S (%)	TS/TOC	Original OM (%)	Silicates (%)	S1 *	S2 *	S3 **	Tmax (°C)	HI ***	OI ****
14/1104	80.04	T	12.27	56.88										
14/1105	80.08	T	11.18	60.41	2.03	0.18	16.62	22.97	1.86	86.11	3.09	412	770	28
14/1106	82.26	T	3.02	90.98										
14/1107	83.16	T	16.69	67.15										
14/1108	84.28	T	17.72	50.71										
14/1109	85.15	T	12.61	66.79	1.97	0.16	18.37	14.84	1.96	91.00	3.00	415	722	24
14/1110	85.95	T	9.78	74.79										
14/1111	87.13	T	9.47	84.79										
14/1112	88.01	T	3.60	93.72										
14/1113	88.7	T	2.63	99.86	0.34	0.13			0.29	22.00	1.23	413	836	47
14/1114	89.81	T	11.59	71.99										
14/1115	91.32	T	13.06	74.41										
14/1116	92.5	T	8.21	84.53										
14/1117	93.2	T	7.91	80.33	1.32	0.17	11.62	8.05	1.00	51.41	1.54	412	650	19
14/1118	94.45	T	11.04	52.93	2.68	0.24	17.16	29.91	1.51	82.47	3.02	414	747	27
14/1119	95.37	T	18.00	65.22										
14/1120	96.41	T	15.97	28.83										
14/1121	97.46	T	15.36	69.32	2.50	0.16	22.50	8.18	2.37	101.19	3.15	412	659	21
14/1122	98.545	T	6.71	79.44										
14/1123	99.3	T	4.56	90.17										
14/1124	99.98	T	12.20	71.24	2.34	0.19	18.26	10.50	1.65	82.99	3.11	408	680	26
14/697	100.09	CT	12.00	70.77	1.86	0.15	17.46	11.77	2.09	82.09	3.04	407	684	25
14/698	100.305	CT	12.79	70.36	2.46	0.19	19.15	10.48						
14/699	100.49	CT	18.44	53.86										
14/700	100.68	CT	9.73	58.03	2.26	0.23	15.01	26.96	1.13	65.37	2.75	411	672	28
14/695	100.69	CT	12.63	47.58	3.53	0.28	20.14	32.27	1.18	79.32	2.84	412	628	23
14/696	100.91	CT	11.49	63.26	2.40	0.21	17.43	19.31						
14/782	100.92	CT	15.44	39.39	4.34	0.28	24.66	35.94	1.88	94.11	3.10	410	609	20
14/701	101.11	CT	12.12	65.34	2.87	0.24	18.76	15.90						
14/702	101.3	CT	11.52	61.42	2.54	0.22	17.62	20.95						
14/703	101.49	CT	14.13	66.76	2.19	0.16	20.58	12.66						
14/783	101.67	CT	12.59	63.63	1.70	0.14	18.05	18.32	2.17	89.47	2.87	412	711	23
14/704	101.7	CT	13.23	62.61										
14/705	101.89	CT	14.19	73.82	1.90	0.13	20.33	5.85						
14/706	102.09	CT	12.13	76.56										
14/707	102.32	CT	8.29	76.61	1.52	0.18	12.34	11.05						
14/784	102.44	CT	7.62	70.52	1.22	0.16	11.13	18.35	1.12	53.95	1.50	413	708	20
14/708	102.53	CT	7.45	67.50	1.35	0.18	11.07	21.43	0.62	46.76	1.62	416	627	22
14/709	102.73	CT	6.74	78.45	1.15	0.17	9.93	11.62						
14/711	103.21	CT	4.43	85.65	1.20	0.27	7.03	7.32	0.48	31.38	1.45	415	708	33
14/712	103.42	CT	4.71	94.69	0.80	0.17								
14/713	103.61	CT	5.50	80.02	1.62	0.29	8.86	11.12	0.58	37.61	1.52	413	684	28
14/785	103.66	CT	6.27	79.40	0.91	0.15	9.07	11.53	0.95	46.55	1.53	412	742	24
14/714	103.81	CT	5.86	95.13	0.89	0.15								
14/786	103.97	CT	9.29	60.11	1.69	0.18	13.80	26.09	1.59	81.09	2.96	411	873	32
14/715	104.02	CT	11.71	75.38	1.68	0.14	16.89	7.73	1.84	94.67	2.94	413	674	21
14/716	104.21	CT	14.04	68.54	2.87	0.20	21.22	10.24						
14/717	104.4	CT	12.71	77.58	1.80	0.14	18.32	4.10						
14/718	104.59	CT	8.05	82.63	1.05	0.13	11.50	5.87	1.11	59.82	3.01	414	743	37
14/719	104.78	CT	7.15	86.62	0.73	0.10	9.99	3.39						
14/720	104.98	CT	3.56	94.55	0.52	0.15	5.15	0.30	0.44	27.46	1.60	414	771	45
14/721	105.18	CT	1.90	108.28	0.32	0.17								
14/722	105.39	CT	5.11	96.35	0.77	0.15								
14/723	105.62	CT	8.04	67.61	1.20	0.15	11.66	20.73	1.13	61.59	3.14	411	766	39
14/787	105.62	CT	8.86	71.44	1.14	0.13	12.64	15.93						
14/724	105.83	CT	6.83	89.76	1.05	0.15	9.94	0.30						
14/725	106.04	CT	2.62	100.10	0.54	0.21								
14/726	106.28	CT	6.77	68.43	1.02	0.15	9.82	21.75	0.91	50.00	1.74	415	738	26
14/788	106.43	CT	7.22	58.00	1.31	0.18	10.73	31.27	0.88	50.33	1.51	412	697	21

TABLE I. (Cont.)

Sample	Depth [m]	Age	TOC (%)	CaCO ₃ (%)	S (%)	TS/TOC	Original OM (%)	Silicates (%)	S1 *	S2 *	S3 **	Tmax (°C)	HI ***	OI ****
14/727	106.45	CT	7.88	61.48	2.18	0.28	12.56	25.96						
14/728	106.63	CT	10.01	65.34	1.79	0.18	14.85	19.81						
14/729	106.83	CT	7.44	65.41	1.47	0.20	11.18	23.41	1.06	53.89	1.75	417	725	24
14/730	107.04	CT	6.68	70.22	1.08	0.16	9.77	20.01						
14/731	107.24	CT	6.45	58.18	1.38	0.21	9.81	32.01	0.92	48.51	1.73	416	752	27
14/732	107.47	CT	5.98	63.62	1.88	0.31	9.77	26.60						
14/789	107.64	CT	5.48	66.07	1.50	0.27	8.71	25.22	0.59	41.41	1.51	413	756	28
14/733	107.67	CT	5.57	67.18	1.56	0.28	8.88	23.93	0.74	43.65	1.72	414	784	31
14/790	107.92	CT	9.22	70.61	1.21	0.13	13.18	16.22						
14/734	108.18	CT	5.82	81.87	0.81	0.14	8.37	9.76						
14/735	108.38	CT	4.23	83.10	0.67	0.16	6.17	10.73	0.62	35.42	1.70	413	837	40
14/736	108.58	CT	3.20	96.56	0.37	0.12								
14/737	108.8	CT	10.41	62.52	1.52	0.15	15.05	22.43	1.85	82.60	3.25	412	794	31
14/738	109	CT	11.37	65.81	1.91	0.17	16.71	17.48						
14/791	109.19	CT	8.37	51.27	1.83	0.22	12.78	35.95	1.09	67.46	3.00	412	806	36
14/739	109.22	CT	6.64	52.24	1.93	0.29	10.68	37.09						
14/740	109.42	CT	5.72	57.37	1.36	0.24	8.85	33.77	0.60	36.22	1.47	413	634	26
14/741	109.64	CT	3.81	75.65	1.13	0.30	6.15	18.20						
14/742	109.85	CT	4.31	68.26	1.07	0.25	6.72	25.02	0.59	36.87	1.78	414	856	41
14/743	109.9	CT	3.81	76.95	0.70	0.18	5.68	17.38						
14/744	110.1	CT	9.40	53.24	1.50	0.16	13.73	33.03	1.07	61.34	2.61	419	653	28
14/745	110.31	CT	9.75	64.00	1.96	0.20	14.70	21.30						
14/792	110.48	CT	8.71	53.98	1.80	0.21	13.19	32.83	1.09	65.42	2.85	413	751	33
14/746	110.51	CT	7.82	51.01	1.75	0.22	11.99	37.01	1.11	56.35	1.77	416	721	23
14/747	110.68	CT	10.39	61.81	2.00	0.19	15.56	22.63						
14/748	110.92	CT	9.09	63.91	1.68	0.18	13.54	22.54	1.69	76.70	3.27	407	844	36
14/749	111.18	CT	7.05	74.87	1.46	0.21	10.68	14.45						
14/793	111.34	CT	10.04	62.87	1.45	0.14	14.50	22.63	1.68	78.17	3.14	411	778	31
14/750	111.42	CT	9.34	61.11	1.76	0.19	13.95	24.94	1.12	63.10	2.79	414	676	30
14/751	111.66	CT	8.67	74.44	1.20	0.14	12.46	13.10						
14/752	111.88	CT	4.77	88.82	0.81	0.17	7.03	4.14						
14/753	112.08	CT	4.48	80.79	0.89	0.20	6.74	12.46	0.53	32.54	1.40	414	726	31
14/794	112.19	CT	8.74	61.28	1.31	0.15	12.68	26.05	1.02	67.11	2.88	411	768	33
14/755	112.56	CT	4.63	90.51	0.72	0.15	6.74	2.74						
14/756	112.76	CT	4.32	91.43	0.61	0.14	6.22	2.34						
14/757	112.95	CT	10.70	41.46	2.28	0.21	16.27	42.27						
14/758	113.21	CT	10.14		1.97	0.19			1.30	72.17	2.67	412	712	26
14/759	113.41	CT	9.72	52.39	1.92	0.20	14.61	33.00						
14/795	113.51	CT	8.82	62.31	1.43	0.16	12.91	24.79	1.07	68.60	2.99	412	778	34
14/760	113.58	CT	8.84	65.89	1.71	0.19	13.25	20.86						
14/761	113.82	CT	8.04	73.92	1.41	0.18	11.89	14.19						
14/762	114.02	CT	2.81	93.45	0.43	0.15	4.08	2.46						
14/763	114.22	CT	1.71	100.14	0.28	0.17								
14/764	114.42	CT	7.00	80.86	1.35	0.19	10.48	8.66						
14/765	114.64	CT	12.74	49.60	2.13	0.17	18.73	31.67						
14/766	114.82	CT	6.03		1.44	0.24			0.63	43.21	1.48	417	716	25
14/767	115.06	CT	4.93	68.28	1.18	0.24	7.65	24.06						
14/584	115.17	UC	4.41	67.67	1.16	0.26	6.95	25.37	0.46	34.32	1.55	415	779	35
14/585	116.11	UC	7.24	64.91	1.58	0.22	11.05	24.03						
14/586	117.03	UC	7.47	47.98	1.77	0.24	11.57	40.45	0.90	51.61	1.60	414	691	21
14/587	118.18	UC	8.13	64.40	1.56	0.19	12.17	23.43						
14/588	118.9	UC	7.29	47.53	2.17	0.30	11.77	40.70	0.84	48.85	1.86	416	670	26
14/589	120.42	UC	3.04	80.05	0.76	0.25	4.75	15.21						
14/590	121.18	UC	6.21	63.31	1.00	0.16	9.08	27.61	0.94	46.25	1.46	416	745	24
14/591	122	UC	4.76	59.46	1.09	0.23	7.32	33.21						
14/592	123.25	UC	5.42	65.06	0.95	0.18	8.02	26.92						
14/593	124.05	UC	8.19	60.63	1.30	0.16	11.96	27.41	1.26	65.12	2.87	415	795	35
14/595	126.155	UC	6.23	55.81	1.04	0.17	9.16	35.04	0.86	46.43	1.47	412	745	24
14/596	127.205	UC	6.84	45.69	1.48	0.22	10.43	43.88						

TABLE I. (Cont.)

Sample	Depth [m]	Age	TOC (%)	CaCO ₃ (%)	S (%)	TS/TOC	Original OM (%)	Silicates (%)	S1 *	S2 *	S3 **	Tmax (°C)	HI ***	OI ****
14/598	129.04	UC	4.23	58.23	1.65	0.39	7.26	34.50						
14/599	130.28	UC	6.40	56.68	1.92	0.30	10.36	32.96	0.73	44.89	1.50	418	701	23
14/600	131.13	UC	5.24	53.37	1.34	0.26	8.21	38.42						
14/601	132.29	UC	5.27	69.61	0.94	0.18	7.82	22.57						
14/602	133.36	UC	6.46	43.42	1.92	0.30	10.44	46.14						
14/603	134.27	UC	7.55	64.54	1.39	0.18	11.24	24.22						
14/604	135.26	UC	6.11	77.37	0.75	0.12	8.67	13.96						
14/605	136.17	UC	5.09	56.37	1.17	0.23	7.84	35.79	0.46	36.26	1.46	414	712	29
14/606	137.09	UC	7.81	37.17	1.72	0.22	11.94	50.89						
14/607	138.44	UC	2.24	78.56	1.27	0.57	4.30	17.14						
14/608	139	UC	5.65	65.77	1.27	0.22	8.67	25.56						
14/609	139.96	UC	3.96	85.16	0.62	0.16	5.77	9.07						
14/610	141.22	UC	5.71	66.87	1.35	0.24	8.83	24.29						
14/611	142.32	UC	8.10	46.28	1.35	0.17	11.90	41.82	1.94	63.80	2.97	417	788	37
14/796	142.7	UC	7.76	56.08	1.63	0.21	11.78	32.14						
14/612	143.22	UC	4.13	54.76	1.35	0.33	6.81	38.42						
14/613	144.48	UC	7.70	70.92	1.24	0.16	11.26	17.82						
14/614	145.46	UC	3.84	77.66	0.77	0.20	5.78	16.56						
14/615	146.63	UC	7.03	63.41	1.14	0.16	10.29	26.30						
14/616	147.66	UC	5.11	39.77	1.28	0.25	7.98	52.24						
14/617	148.43	UC	5.29	43.96	1.37	0.26	8.32	47.72	0.54	35.56	1.49	414	673	28
14/618	149.52	UC	6.07	35.47	1.44	0.24	9.40	55.13						
14/619	150.23	UC	4.40	79.04	0.75	0.17	6.48	14.48						
14/621	154	UC	4.04	78.09			5.19	16.73						
14/622	156.33	UC	4.39	74.58			5.63	19.79						
14/623	158.11	UC	4.80	63.56	0.87	0.18	7.12	29.32	0.99	35.91	1.47	415	749	31
14/624	160.12	UC	3.64											
14/625	162.35	UC	3.73											
14/628	168	UC	5.35	45.48	2.01	0.38	9.12	45.40	0.48	35.18	1.62	414	657	30
14/631	174.59	UC	2.56											
14/632	176.31	UC	7.88											
14/633	178.3	UC	4.78	55.43	1.10	0.23	7.36	37.21	0.54	32.36	1.56	416	677	33
14/638	187.92	UC	2.98	35.01	1.87	0.63	5.92	59.07	0.20	16.19	1.39	427	543	47
14/643	198.69	UC	3.39	25.97	1.06	0.31	5.54	68.49	0.40	22.20	1.54	420	654	46
14/644	200.69	UC	2.68	41.14			3.43	55.43						
14/645	202.13	UC	4.10	41.49			5.26	53.25						
14/647	206.83	UC	4.99											
14/648	208.5	UC	4.91	55.27	0.94	0.19	7.35	37.38	0.40	31.47	1.43	422	641	29
14/649	210.42	UC	5.63											
14/653	218.74	UC	5.42	36.64	1.05	0.19	8.12	55.24	0.47	34.04	1.66	418	628	31
14/658	228.07	LS	2.70	56.70	0.67	0.25	4.21	39.09	0.30	18.11	1.58	416	672	59
14/663	238.58	LS	2.36	49.85	0.70	0.29	3.81	46.34	0.21	12.37	1.45	425	524	62
14/668	248.26	LS	1.50	28.84	1.23	0.82	3.30	67.85	0.26	4.44	1.21	424	295	81
14/673	258.24	LS	2.12	51.54	0.55	0.26	3.32	45.13	0.13	9.95	1.53	425	471	72
14/678	268.5	LS	4.36	40.85	0.87	0.20	6.58	52.58	0.28	18.11	1.67	423	415	38
14/684	280.1	LS	1.38	20.82	0.42	0.30	2.24	76.94	0.08	4.41	1.58	427	319	114
14/689	290.23	LS	2.02	17.21	0.95	0.47	3.66	79.14	0.14	7.87	1.52	422	389	75
14/694	300.2	LS	1.85	40.04	0.71	0.38	3.17	56.80	0.11	6.43	1.46	423	347	79
14/768	305.3	LS	1.86	50.47	0.53	0.29	2.99	46.55	0.11	7.42	1.19	424	398	64
14/770	315.14	LS	3.04	37.00			3.90	59.11	0.23	21.17	1.39	417	697	46
14/771	320.34	LS	4.54	73.29	0.70	0.15	6.60	20.11	0.47	29.05	1.49	417	640	33
14/772	325.77	LS	2.54	29.22	0.94	0.37	4.31	66.47	0.16	12.71	1.43	423	501	57
14/774	335.33	LS	0.82	37.84	0.55		1.67	60.49	0.06	1.51	1.27	424	208	176
14/776	345.055	LS	3.09	20.05	1.55	0.50	5.70	74.25	0.14	11.22	1.52	424	363	49
14/777	350.03	A	4.19	54.60	0.67	0.16	6.12	39.29	0.31	25.83	1.54	418	617	37
14/778	350.19	A	6.37	53.35	1.07	0.17	9.36	37.29	0.57	40.06	2.01	420	629	31

* mgHC/Rock

** mgCO₂/gRock

*** mgHC/gTOC

**** mgCO₂/gTOC

UC upper Cenomanian

LC lower Cenomanian

T Turonian

CT CTBE

A Albian

TABLE II. XRF data of selected samples from each stratigraphic units

Sample	Depth (m)	Age	SiO ₂	Fe ₂ O ₃ (T)	TiO ₂	Al ₂ O ₃	MnO
14/1077	53.52	Turonian	23.25	1.48	0.20	2.95	0.02
14/1113	88.7	Turonian	3.78	0.10	0.02	< 0,4	0.01
14/1117	93.2	Turonian	5.54	0.31	0.04	< 0,4	0.01
14/1118	94.45	Turonian	19.98	1.55	0.09	2.12	0.01
14/782	100.92	CTBE	14.18	3.64	0.31	4.98	0.02
14/784	102.44	CTBE	9.58	0.54	0.06	1.20	0.01
14/794	112.19	CTBE	19.94	1.07	0.19	3.10	0.01
14/763	114.22	CTBE	6.91	0.11	0.02	< 0,4	0.02
14/766	114.82	CTBE	27.04	1.42	0.27	3.81	0.02
14/587	118.18	Upper Cenomanian	13.57	1.20	0.11	2.07	0.01
14/598	129.04	Upper Cenomanian	25.04	2.54	0.30	4.22	0.02
14/619	150.23	Upper Cenomanian	12.67	0.99	0.12	1.81	0.02
14/628	168	Upper Cenomanian	20.59	1.83	0.27	4.74	0.02
14/638	187.92	Upper Cenomanian	30.10	4.82	0.41	9.12	0.04
14/654	220.57	Lower Cenomanian	27.18	1.38	0.39	4.47	0.02
14/668	248.26	Lower Cenomanian	48.34	4.47	0.61	6.82	0.02
14/678	268.5	Lower Cenomanian	23.92	3.09	0.40	10.09	0.03
14/768	305.3	Lower Cenomanian	25.25	4.15	0.35	7.74	0.04
14/772	325.77	Lower Cenomanian	45.55	2.84	0.52	6.93	0.03
14/776	345.06	Lower Cenomanian	42.14	5.15	0.52	12.64	0.02

Sample	Depth (m)	Age	MgO	CaO	Na ₂ O	K ₂ O	P ₂ O ₅
14/1077	53.52	Turonian	4.07	28.45	< 0,2	0.23	0.30
14/1113	88.7	Turonian	0.33	52.19	< 0,2	0.01	0.08
14/1117	93.2	Turonian	0.39	46.08	< 0,2	0.01	0.07
14/1118	94.45	Turonian	0.30	33.28	< 0,2	0.24	0.33
14/782	100.92	CTBE	0.20	27.82	< 0,2	0.36	0.04
14/784	102.44	CTBE	0.25	43.39	< 0,2	0.01	0.06
14/794	112.19	CTBE	0.47	34.99	< 0,2	0.17	0.05
14/763	114.22	CTBE	0.55	73.64	< 0,2	0.01	0.11
14/766	114.82	CTBE	0.73	31.82	< 0,2	0.46	0.10
14/587	118.18	Upper Cenomanian	0.32	39.47	< 0,2	0.01	0.06
14/598	129.04	Upper Cenomanian	3.22	30.04	< 0,2	0.27	0.44
14/619	150.23	Upper Cenomanian	0.94	42.91	< 0,2	0.01	0.06
14/628	168	Upper Cenomanian	0.98	34.56	0.23	0.81	1.46
14/638	187.92	Upper Cenomanian	4.65	19.07	< 0,2	3.09	0.20
14/654	220.57	Lower Cenomanian	0.85	45.86	< 0,2	0.45	1.78
14/668	248.26	Lower Cenomanian	2.01	16.07	0.60	1.18	0.31
14/678	268.5	Lower Cenomanian	1.48	28.49	0.29	0.65	0.23
14/768	305.3	Lower Cenomanian	2.44	27.76	< 0,2	1.59	0.23
14/772	325.77	Lower Cenomanian	1.73	19.34	< 0,2	2.02	0.17
14/776	345.06	Lower Cenomanian	1.92	13.62	1.10	1.97	0.21

Sample	Depth (m)	Age	SO ₃	LOI	Total
14/1077	53.52	Turonian	5.83	33.03	99.88
14/1113	88.7	Turonian	< 0,2	42.26	99.18
14/1117	93.2	Turonian	2.54	44.07	99.31
14/1118	94.45	Turonian	4.53	36.88	99.38
14/782	100.92	CTBE	9.67	38.01	99.28
14/784	102.44	CTBE	2.70	41.82	99.67
14/794	112.19	CTBE	2.13	36.90	99.09
14/763	114.22	CTBE	< 0,2	17.15	99.00
14/766	114.82	CTBE	2.11	31.52	99.35
14/587	118.18	Upper Cenomanian	3.08	39.50	99.45
14/598	129.04	Upper Cenomanian	2.98	30.19	99.33
14/619	150.23	Upper Cenomanian	1.33	38.11	99.03
14/628	168	Upper Cenomanian	4.72	28.77	98.98
14/638	187.92	Upper Cenomanian	3.77	23.24	98.59
14/654	220.57	Lower Cenomanian	1.11	15.70	99.26
14/668	248.26	Lower Cenomanian	2.71	16.47	99.63
14/678	268.5	Lower Cenomanian	1.23	29.60	99.49
14/768	305.3	Lower Cenomanian	0.67	29.60	99.88
14/772	325.77	Lower Cenomanian	0.75	19.39	99.33
14/776	345.06	Lower Cenomanian	1.52	17.88	98.67